



Australian Journal of Earth Sciences

An International Geoscience Journal of the Geological Society of Australia

ISSN: 0812-0099 (Print) 1440-0952 (Online) Journal homepage: <http://www.tandfonline.com/loi/taje20>

Origin and evolution processes of hybrid event beds in the Lower Cretaceous of the Lingshan Island, Eastern China

T. Yang, Y. Cao, H. Friis, K. Liu & Y. Wang

To cite this article: T. Yang, Y. Cao, H. Friis, K. Liu & Y. Wang (2018) Origin and evolution processes of hybrid event beds in the Lower Cretaceous of the Lingshan Island, Eastern China, Australian Journal of Earth Sciences, 65:4, 517-534, DOI: [10.1080/08120099.2018.1433236](https://doi.org/10.1080/08120099.2018.1433236)

To link to this article: <https://doi.org/10.1080/08120099.2018.1433236>



Published online: 16 May 2018.



Submit your article to this journal [↗](#)



Article views: 9






View related articles [↗](#)



View Crossmark data [↗](#)

Origin and evolution processes of hybrid event beds in the Lower Cretaceous of the Lingshan Island, Eastern China

T. Yang ^{a,b,c}, Y. Cao ^a, H. Friis^c, K. Liu ^a and Y. Wang^a

^aSchool of Geosciences, China University of Petroleum, Qingdao, 266580, PR China; ^bShandong Provincial Key Laboratory of Depositional Mineralization & Sedimentary Minerals, Shandong University of Science and Technology, Qingdao 266580, Shandong, PR China; ^cDepartment of Geoscience, Aarhus University, Høegh-Guldbergs Gade 2, DK-8000 Aarhus C, Denmark

ABSTRACT

On the basis of detailed sedimentological investigation, three types of hybrid event beds (HEBs) together with debrites and turbidites were distinguished in the Lower Cretaceous sedimentary sequence on the Lingshan Island in the Yellow Sea, China. HEB 1, with a total thickness of 63–80 cm and internal bipartite structures, is characterised by a basal massive sandstone sharply overlain by a muddy sandstone interval. It is interpreted to have been formed by particle rearrangement at the base of cohesive debris flows. HEB 2, with a total thickness of 10–71 cm and an internal tripartite structure, is characterised by a normal grading sandstone base, followed by muddy siltstone middle unit and capped with siltstones; the top unit of HEB 2 may in places be partly or completely eroded. The boundary between the lowest unit and the middle unit is gradual, whereas that between the middle unit and the top unit is sharp. HEB 2 may be developed by up-dip muddy substrate erosion. HEB 3, with a total thickness up to 10 cm and an internal bipartite structure, is characterised by a basal massive sandstone sharply overlain by a muddy siltstone interval. The upper unit was probably deposited by cohesive debris flow with some plant fragments and rare mud clasts. HEB 3 may be formed by the deceleration of low-density turbidity currents. The distribution of HEBs together with debrites and turbidites implies a continuous evolution process of sediment gravity flows: debris flow → hybrid flow caused by particle rearrangement → high-density turbidity current → hybrid flow caused by muddy substrate erosion → low-density turbidity current → hybrid flow caused by deceleration.

ARTICLE HISTORY

Received 13 September 2017
Accepted 15 January 2018

KEYWORDS

turbidity current; debris flow; hybrid even beds; evolution processes; Lower Cretaceous; Lingshan Island

Introduction

Deep-water sediment gravity flows, which are one of the most important sediment transport mechanisms on Earth (Mulder & Alexander, 2001; Talling et al., 2015; Yang, Cao, Wang, Li, & Zhang, 2015), can form thick and large sand bodies of coarse-clastic and associated fine-grained sediments in both marine and lacustrine environments (Stow & Johansson, 2000; Stow & Mayall, 2000; Yang, Fan, Han, & Van Loon, 2017b; Yang, Jin, Van Loon, Han, & Fan, 2017a). Understanding the origin of deep-water sediment gravity flows is critical for predicting the distribution of deep-water oil and gas reservoirs, protecting strategic submarine communication cable networks against potential hazards, and determining the recurrence periods of natural disasters such as earthquakes (Talling, Paull, & Piper, 2013). There is a comprehensive process referred to as 'triggering-transportation-deposition' of deep-water sediment gravity flow to form a deep-water sandstone, which is also called a deep-water sediment gravity-flow event (Talling, Masson, Sumner, & Malgesini, 2012). The development of deep-water sediment gravity flows and their transformation

into different flow types constituting one deep-water sediment gravity-flow event can form hybrid event beds (HEBs) (e.g. Felix & Peakall, 2006; Hampton, 1972; Haughton, Barker, & McCaffrey, 2003; Mutti, Tinterri, Remacha, & Fava, 1999; Talling, 2013; Talling, Amy, Wynn, Peakall, & Robinson, 2004). HEBs refer to the deposits of mixed deep-water sediment gravity flows in a single sediment gravity-flow event, which contains turbidity currents, debris flows and occasionally transitional flows (Haughton, Davis, McCaffrey, & Barker, 2009; Talling, 2013). The idea of HEBs was inspired from the previous research works related to slurry-flow deposits (Lowe & Guy, 2000; Lowe, Guy, & Palfrey, 2003), linked debrites (Haughton et al., 2003), and cogenetic debrite–turbidite beds (Talling et al., 2004). Linked debrites and cogenetic debrite–turbidite beds are previously used to describe a bed (HEB) composed of both turbidites and debrites (Haughton et al., 2003; Talling et al., 2004). Slurry-flow deposits are characterised by light and dark bands, and were interpreted as deposited by sediment gravity flows, which are transitional between debris flows and turbidity currents (Lowe & Guy, 2000; Lowe et al., 2003). Thus, slurry flow deposits have also

been referred as transitional flow deposits (Kane & Pontén, 2012; Lowe & Guy, 2000; Yang et al., 2017b). Since slurry flows have also been used to refer to plastic flows with a similar behaviour in respect to debris flows, Haughton et al. (2009) recommended slurry-flow deposits to be considered as a HEB variant. Much work has been carried out on outcrops (e.g. Fonnesu, Haughton, Felletti, & McCaffrey, 2015; Fonnesu, Patacci, Haughton, Felletti, & McCaffrey, 2016; Ito, 2008; Jackson, Zakaria, Johnson, Tongkul, & Crevello, 2009; McCaffrey & Kneller, 2001; Patacci, Haughton, & McCaffrey, 2014; Talling et al., 2004; Tinterri & Muzzi Magalhaes, 2011; Wood & Smith, 1959), cores (e.g. Haughton et al., 2003, 2009; Lowe & Guy, 2000; Lowe et al., 2003; Southern, Kane, Warchol, Porten, & McCaffrey, 2017), sonar scan images (Lee et al., 2013), flume experiments (Baas, Best, & Peakall, 2011; Baas, Best, Peakall, & Wang, 2009; Sumner, Talling, & Amy, 2009), numerical simulations (Amy, Peachey, Gardiner, & Talling, 2009) and geophysical features (Georgiopoulou, Wynn, Masson, & Frenz, 2009) to analyse the sedimentary characteristics, origins and distribution patterns of HEBs. HEBs mainly comprise a basal turbidite clean sandstone overlapped by mud-rich debrite sandstone bounded by a sharp or gradual boundary (Haughton et al., 2009; Talling, 2013). The transitional flows between debris flows and turbidity currents form stacked light and dark 'bands' (Haughton et al., 2009; Lowe & Guy, 2000), which may sometimes occur between turbidite and debrite of HEBs. The lateral continuity of HEBs with uniform thickness and their regular repetitive nature indicate an origin related to one sediment gravity-flow event (Fonnesu et al., 2015; Haughton et al., 2009). Haughton et al. (2009) suggested a five-part (H1–H5) standard depositional sequence of HEBs. The H1 division is the basal thick clean sandstones deposited by turbidity currents, being always structureless, graded-to-ungraded, and in places containing dewatering structures (Fonnesu et al., 2015). The H2 division is characterised by stacked lighter and darker 'bands' formed by transitional flows (Lowe & Guy, 2000). The H3 division is the deposits of debris flows with abundant mud clasts, or in places having abundant mud matrix instead of mud clasts (Talling, 2013). The H4 division is thin-bedded sandstone with ripple cross-lamination deposited by low-density turbidity currents. The H5 division is the massive mudstones formed by low-density turbidity currents. Elsewhere, the H2 divisions may be poorly developed and can be easily overlooked (Fonnesu et al., 2015; Talling, 2013). In other cases, the H2 divisions may dominate the deposition succession forming lighter and darker 'bands' of metres to tens of metres thick (Fonnesu, Felletti, Haughton, Patacci, & McCaffrey, 2018; Haughton et al., 2009; Lowe & Guy, 2000; Lowe et al., 2003; Southern et al., 2017). The H4 may be absent, or may entirely or partly have collapsed into the underlying H3 division, making it difficult to identify (Fonnesu et al., 2015). The origin of HEBs is related to different transport and settling processes, which result in turbidites being covered by debrites (Haughton et al., 2009; Talling, 2013), the late-stage settling of sand from the debris flow plug (Sumner et al., 2009; Talling, 2013; Talling et al., 2004), conversion from turbidity currents into debris flows by

muddy substrate erosion (e.g. Haughton et al., 2003, 2009; Haughton, Davis, McCaffrey, & Barker, 2010; Ito, 2008; Kane & Pontén, 2012; Lee et al., 2013; Talling, 2013; Talling et al., 2004), deceleration and expansion (McCave & Jones, 1988), local margin failure in turbidity currents (Haughton et al., 2003, 2009, 2010; Talling, 2013; Talling et al., 2004), local substrate delamination (Fonnesu et al., 2016), and reversing buoyancy in turbidity currents (Pritchard & Gladstone, 2009).

HEBs are always found in the distal part of deep-water basins (Haughton et al., 2003, 2009; Lowe & Guy, 2000; Lowe et al., 2003; Talling et al., 2004, 2007), which is quite different from the traditional distribution model put forward by Mutti et al. (1999). Recently, many researchers have paid great attention to this research field (e.g. Fonnesu et al., 2018; Haughton et al., 2003, Haughton et al., 2009; Kane & Pontén, 2012; Lowe & Guy, 2000; Lowe et al., 2003; Southern et al., 2017; Talling et al., 2004), but the origin and distribution of HEBs are still debated (Higgs, 2010; Talling, 2013). First, we want to know the specific origin of HEBs. Is there only one origin or various geneses corresponding to the different sedimentary features of HEBs? Whether different stages of sediment gravity-flow transportation and deposition or the location correspond to different origins (Felix et al., 2009)? Second, we consider the spatial distribution of the HEBs. Much attention has been paid to the vertical combination according to core and outcrops (Haughton et al., 2009), but limited information is known about the restrictions and conditions of the lateral distribution along sediment gravity-flow evolution process paths (Fonnesu et al., 2015, 2018).

The Lower Cretaceous Fajiyin Formation (Laiyang Group) located on the Lingshan Island, in the Yellow Sea is composed of a typical succession of deep-water sediment gravity-flow deposits (Lu, Wang, & Zhang, 2011; Shao et al., 2014a, 2014b). Previous research has focused on the stratal features (Zhang et al., 2013), sedimentary settings (e.g. Lu et al., 2013; Zhong, 2012; Zhou, Zhang, Liang, Li, & Yue, 2015a), origin and characteristics of soft-sediment deformation structures (e.g. Lu et al., 2011; Yang & Van Loon, 2016), origin and distribution of slump layers (e.g. Dong et al., 2013; Ge, Zhong, Fan, Ren, & Shao, 2015; Lu et al., 2011) and the origin and types of deep-water sediment gravity flows (Shao et al., 2014b). It has been assumed that sediment failure caused these deep-water sediment gravity-flow deposits, which are composed mainly of sandy slumps deposits, sandy debris flow deposits and turbidity current deposits on the Lingshan Island (Shao et al., 2014b). Various kinds of soft-sediment deformation structures at different scales are also common in the deep-water sediment gravity-flow deposits (e.g. Lu et al., 2011; Shao et al., 2014a; Wang, Zhou, Zhang, Yu, & Wang, 2014a; Yang & Van Loon, 2016; Zhou et al., 2015b). The sedimentary environment and the prototype basin of the deep-water sediment gravity-flow deposit in the research areas is still being debated (Lu et al., 2011, 2013; Shao et al., 2014b; Zhang et al., 2013; Zhong, 2012; Zhou et al., 2015a). Zhong (2012) and Shao et al. (2014b) found carbonised plant debris, a band of vitrain and sand-particle imbricate structure in deposits on the Lingshan Island, which indicated the input of terrestrial components to the

deep-water sediment gravity flows in the front of a prograding delta. Lu et al. (2011) believe that the large slump structures are the typical expression of the deep-marine environment, which indicated a remnant ocean basin between the South China Block and the North China Block. The occurrence of fragments of marine dinoflagellate cysts and membranous algae in the Lingshan Island outcrop indicate a marine depositional environment (Zhang et al., 2013). Zhou et al. (2015a) identified a series of parallel marine rift basins from southeast to northwest direction between the uplift and Qianliyan uplift near the coast in East China. More recently, Yang, Fan, Han, and Van Loon (2017c) believed that the research area was in a deep-sea environment based on evidence from trace elements. The discovery of fish and conchostracan fossils in the deep-water sediment gravity-flow deposits offers some strong evidence to support the interpretation of a lacustrine basin environment (Li et al., 2017).

In the study area, several widespread HEBs have been recognised in deep-water sediment gravity-flow sandstones. The aim of this study is to distinguish and analyse the different types of HEBs according to the thickness of the sediment units, sedimentary structures and bounding relationships, and then try to clarify their origin and distribution. From the distribution pattern of HEBs together with the distribution of debrites and turbidites, the evolution process of deep-water sediment gravity flows is discussed.

Geological background

Lingshan Island sag

The Lingshan Island lies in the Yellow Sea, about 10 km offshore Qingdao in east China (Figure 1). The island with maximum altitude of 513.6 m is the highest island in northern China and covers an area of 7.66 km² (Lu et al., 2011) (Figure 1b). Tectonically, the island is in the Lingshan Island sag, a late Mesozoic rift basin between Jiaonan uplift and Qianliyan uplift (Zhou et al., 2015a) (Figure 1b). The Lingshan Island sag is bordered by the Tan-Lu Fault to the west, by the Wulian-Yantai Fault to the north, and by the Qianliyan Fault to the south (Figure 1b). The sag experienced three major tectonic development stages: (1) an initial stage of rifting and subsidence in the beginning of the Early Cretaceous, (2) a stage of slight inversion compression in the middle of the Early Cretaceous and (3) a stage of intense rifting and subsidence towards the end of the Early Cretaceous (Zhou et al., 2015a). After that, the sag underwent intense compression and deformation, resulting in an exposed succession with most strata inclined towards the NEE (Luan, Li, Wang, Li, & Xie, 2010) (Figure 1c).

Stratigraphy

From base to top, two main rock units are exposed along the coastline of the island (Figure 2). Unit 1 is composed mainly of interbedded grey mudstones and massive deep-water sediment gravity-flow sandstones deposits with variable

thickness. Sediment slumps and soft-sediment deformation structures are also common. At the top of this unit, there are some sediment gravity-flow channel-fill and delta-front deposits (Zhong et al., 2016) (Figure 2). The U–Pb ages of detrital zircon derived from the syndepositional volcanic rocks indicate that these deep-water sediment gravity flows were deposited in Unit 1 between 138 and 121 Ma (Wang, Chang, Lu, & Zhang, 2014b), which is coeval with the Fajiyin Formation of the Laiyang Group in the Lower Cretaceous. Zhang et al. (2013) found that Unit 1 on the Lingshan Island is different from other deposits found in the Fajiyin Formation, and have differentiated this unit and named it as the Lingshandao Formation. Deep-water sediment gravity-flow deposits in Unit 1 are mainly found in the outcrop Section A (35°44′51.36″N, 120°9′44.64″E), Section B (35°44′39.26″N, 120°9′44.92″E), Section C (35°45′50.13″N, 120°9′43.53″E), and Section D (35°47′03.74″N, 120°10′29.38″E) (Figures 1c and 2).

The deposits in Section A are composed mainly of interbedded thin-bedded sandstone and mudstones accumulated by low-density turbidity currents. Deposits in Section B are composed mainly of interbedded medium-bedded sandstones and mudstones probably accumulated by high-density turbidity currents (Shao et al., 2014b). The deposits in Section C are composed mainly of thick-bedded debrites, thin-bedded turbidites, and slump deposits with various types of soft-sediment deformation structures (Lu et al., 2011; Shao et al., 2014b). The deposits in Section D are dominated by sediment gravity-flow channel-fill deposits and levee and delta-front channel-fill deposits (Zhong et al., 2016). From base to top, the Lingshandao Formation is composed of a shallowing-upward progradational sequence recognised along the A, B, C, and D sections (Figure 2) (Yang & Van Loon, 2016; Zhou et al., 2015a).

From the lower to the upper part of the succession, Unit 2 is composed mainly of grey–white rhyolite, fan-delta deposits and volcanoclastic breccia (Figure 2). The massive grey–white rhyolite is formed close to 119.2 Ma (Zhou et al., 2015a) (Figure 2). There is an unconformable contact between the Laiyang and the Qingshan groups (Zhou et al., 2015a). Thus, this unit belongs to the Bamudi Formation of the Qingshan Group in the Lower Cretaceous (Wang et al., 2014b; Zhou et al., 2015a). These grey–white rhyolites are mainly exposed in the southwestern part of the island with a thickness range from 0 to 20 m (Figure 1c). The middle section of this unit consists of middle to thick-bedded medium to coarse-grained sandstones together with volcanoclastic rock deposits and lavas. The sandstones are mainly of fan-delta deposits with trough crossing bedding and parallel lamination, as best seen in Section E (35°45′17.35″N, 120°11′01.27″E) (Figures 1c and 2). The top of this unit consists of more than 100 m of massive volcanoclastic breccia that covered almost the entire island (Lu et al., 2011; Zhou et al., 2015a) (Figures 1 and 2).

Methods and terminology

In this study, the deep-water sediment gravity-flow deposits from the outcrop sections A, B and C were investigated in

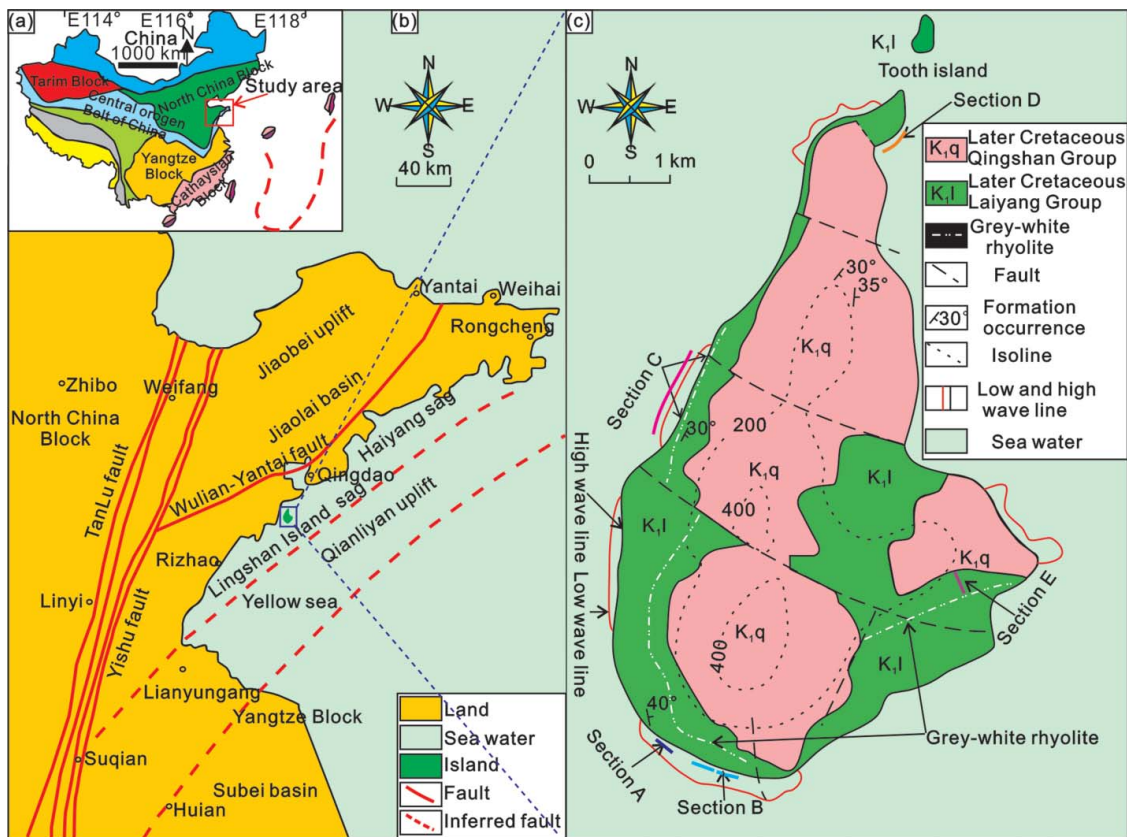


Figure 1. Geological maps and regional stratum distribution in the Lingshan Island. (a) Structural subdivision of China and the location of the study area (modified after Wang et al., 2014a). (b) Geological map and tectonic subdivision of East Shandong (modified after Ge et al., 2015). (c) Geological map of Lingshan Island showing the location of studied sections.

detail. The outcrops are well exposed and easy accessible, and the lateral context of the stratigraphic interval is clear in each section. Individual sections were measured in detail, and composite logs were drawn at a scale of 1:20 (Figure 2). Photomosaics have been used to capture the large-scale distribution of the deep-water sediment gravity-flow sandstones. The thickness and lithology including colour, particle size and mud content, sedimentary structures and vertical organisation of sandstone beds were also recorded in detail. Photos and sketches of representative sedimentary structures and distribution characteristics were captured. Paleocurrent directions were measured in the field primarily on the flute casts. A number of samples have been taken to represent the variations of sandstone and shale lithologies in all outcrop sections. Thirty-three thin-sections were studied under the petrographic microscope to quantify the mud content and determine grain sizes of the samples. The results of microscope analysis were used to refine the observation of fieldwork.

In this paper, we use the term low-density turbidity current to describe the flow in which sediment grains are supported by the turbulent fluid (Talling et al., 2012), differing from high-density turbidity currents, in which grains are supported by hindered setting and grain interactions. Cohesive debris flow is used to describe flows with high mud matrix contents, which can prevent sand settling and deposition from

cohesive freezing (Talling et al., 2012). Poor cohesive debris flows have less mud matrix and the sediment grains are supported by excess pore pressure, buoyancy and grain to grain interaction (Talling et al., 2012). The terms bipartite and tripartite are used to describe the vertical organisation of different flows within the same sediment gravity-flow event as well as their deposits (Mutti, Tinterri, Benevelli, Biase, & Cavanna, 2003).

Results

Petrography

Clean sandstones, muddy siltstones/siltstones, and mudstones could be recognised according to field observations and laboratory analysis (Figure 3). Clean sandstones are mainly composed of fine-grained sandstone and siltstone with low content of mud matrix (10–15%). The colours of clean sandstones are grey and white, reflecting a relatively low mud content. The detrital grains are subangular to sub-rounded (Figure 3a). Clean sandstones are composed mainly of massive sandstones and graded sandstones. The muddy siltstones/siltstones are generally more fine-grained than the clean sandstones. The colour is mainly dark grey, reflecting a relatively high mud content. The detrital grains of the poorly

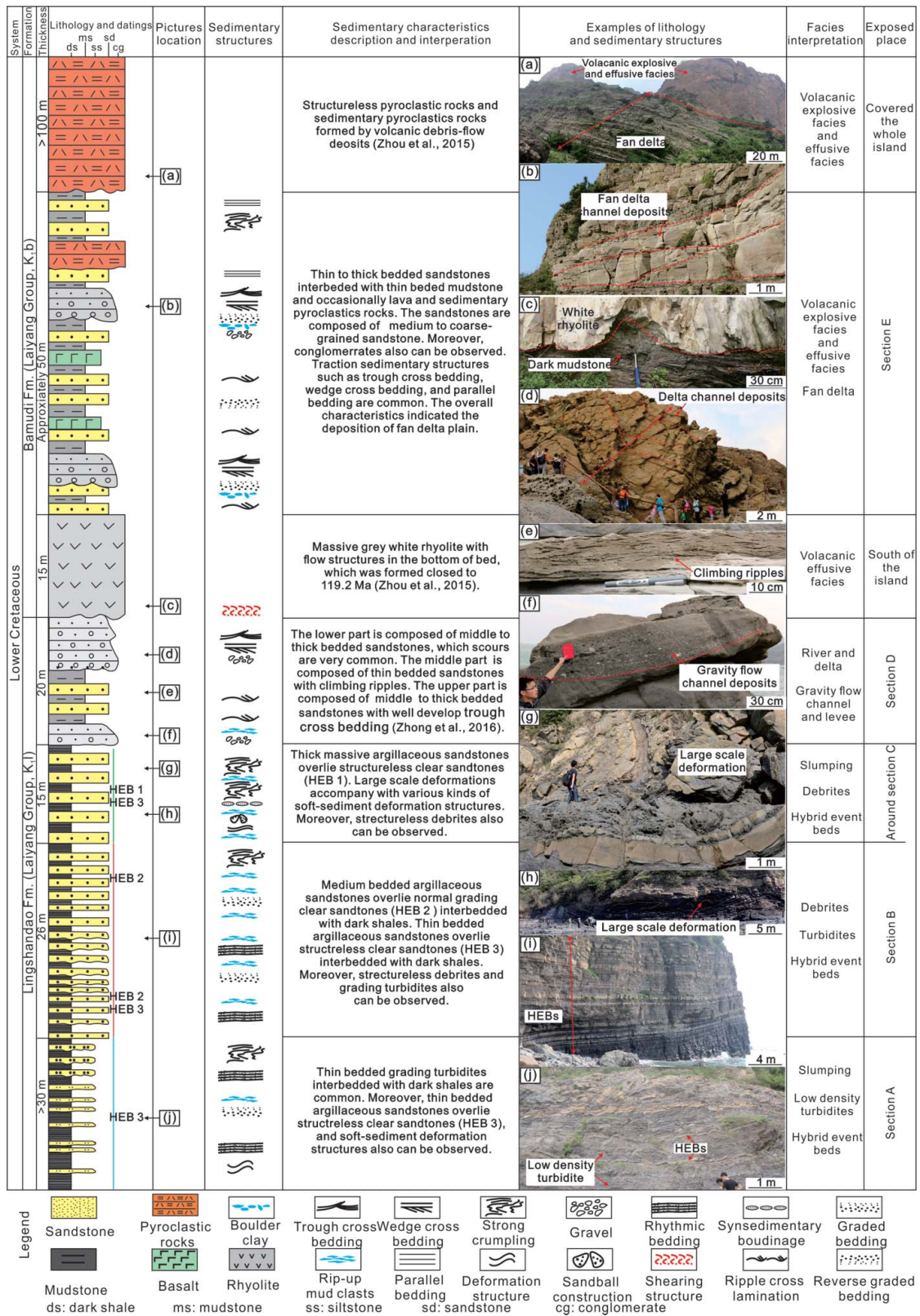


Figure 2. Composed stratigraphic column integrated from different outcropped sections on Lingshan Island (modified after Zhou et al., 2015a).

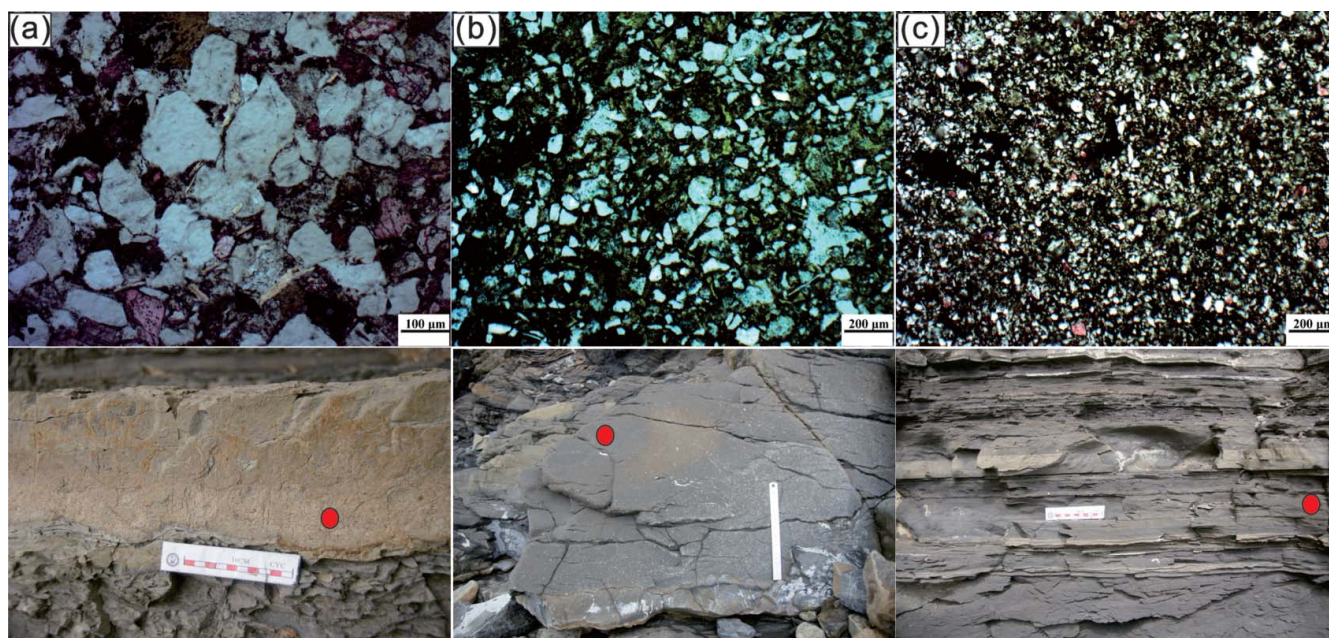


Figure 3. Petrographic characteristics of deep-water sandstones and mudstones from Lingshan Island. Top, photomicrograph; bottom, outcrop photo with location of thin-section sample. (a) Fine-grained sandstones, characterised by subangular or angular shape detrital grains with little mud matrix from section B; (b) mud siltstone with abundant mud matrix and mica from section C; and (c) mudstones with high calcite content from section B.

sorted massive muddy siltstones are subangular to subrounded (Figure 3b). In the exposures, the colour of the sandstones appears brownish yellow owing to weathering. The colour of the mudstones is mainly dark grey with some being brownish black because of the high total organic carbon content. Under the microscope, mica is seen to be parallel to the beddings. Lime mud matrix is abundant in mudstones (Figure 3c).

Paleoflow

Flute casts are well developed at the base of some turbidite sandstones (Figure 4a). The paleocurrent directions from 80 flute casts measured indicate a northeast-to-southwest direction (Figure 4b).

Bed types

Type A beds: massive sandstone beds

Description: Type A beds, usually ranging between 0.1 and 0.8 m, are composed mainly of fine-grained clean sandstone and muddy siltstone. Massive clean sandstone beds in places show floating mud clasts in the middle and upper part of the bed. These beds are usually sharply bounded by mudstones at both the base and the top (Figure 5a) with erosion features rare at the base of the massive clean sandstone beds. Massive muddy siltstone beds are characterised by abundant floating mud clasts and have sharp contacts with the basal and upper mudstones (Figure 5b). Mud clasts can occur in any parts within the muddy siltstones, which are generally randomly

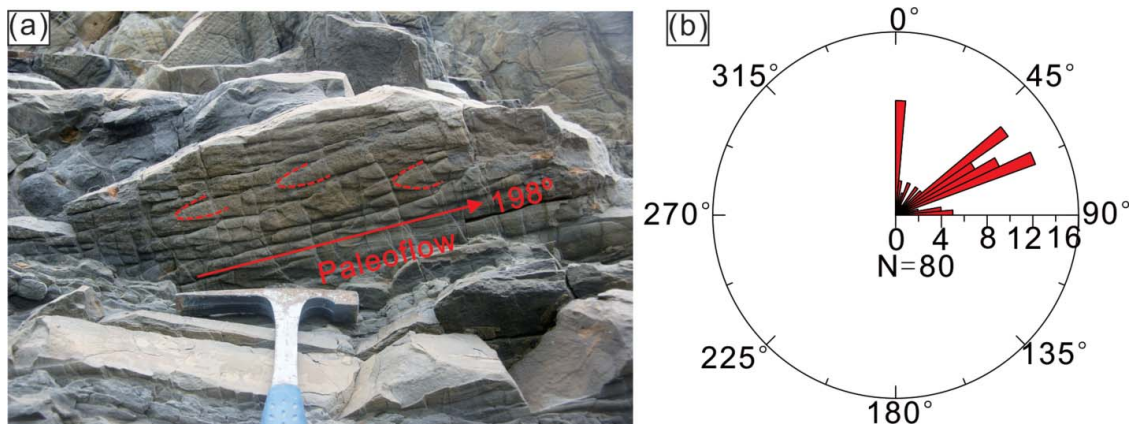


Figure 4. Paleoflow direction measurements in deep-water sediment gravity-flow sandstones from Lingshan Island. (a) Flute casts at the base of turbidite sandstones indicating the direction of paleoflow approximately 198° (hammer for scale is ~22 cm long). (b) Rose diagram showing the paleoflow direction.

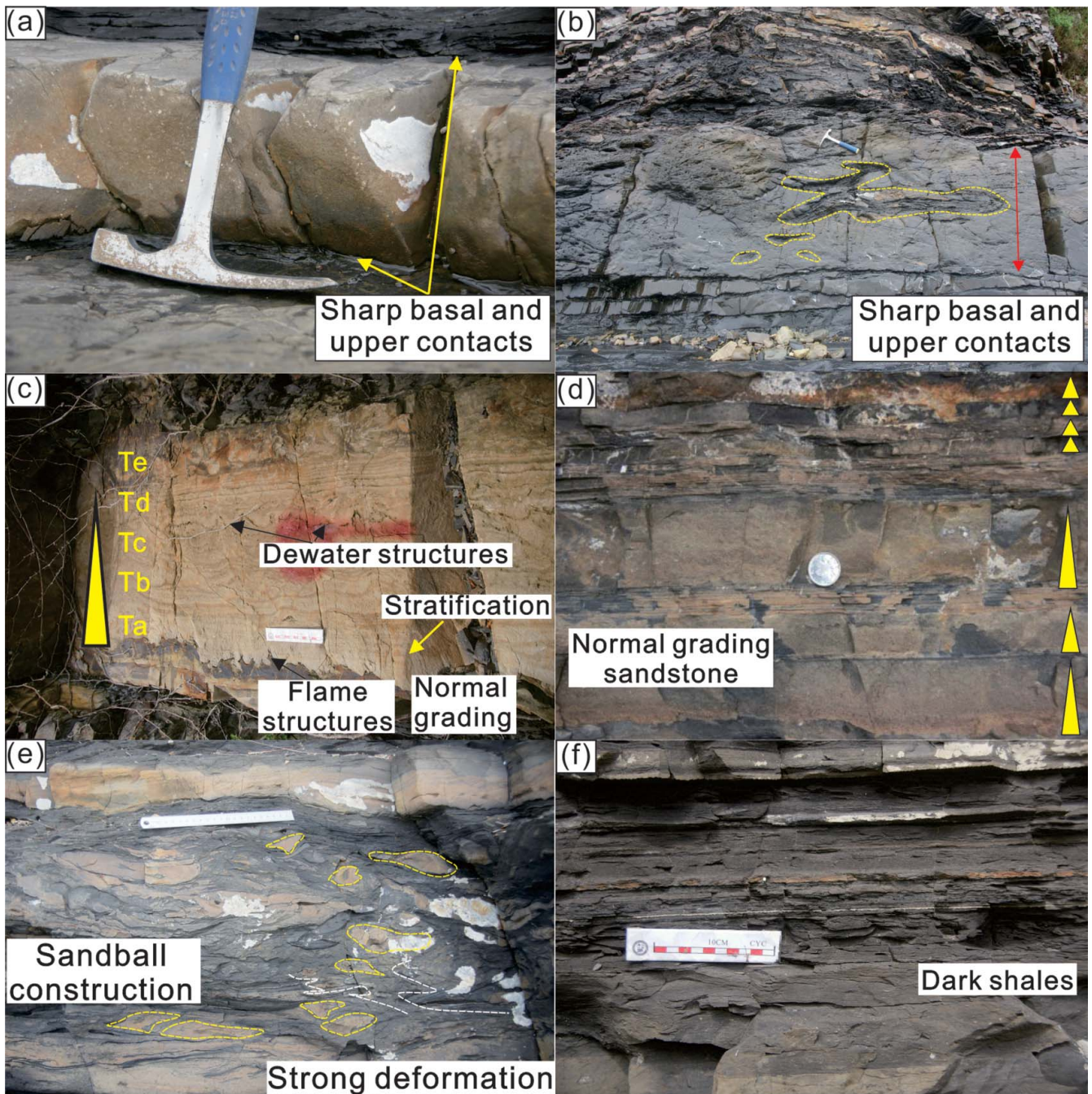


Figure 5. Typical sedimentary structures of deep-water sediment gravity-flow sandstones from the Lingshandao Formation. (a) Massive sandstones interpreted as sandy debrites (hammer for scale is ~22 cm long); (b) muddy debrites with floating mud clasts (hammer for scale is ~22 cm long); (c) Bouma sequence from Ta to Te, showing typical stratification in Ta division (scale is 10 cm); (d) thin-bedded normal-graded sandstones interbedded with mudstones (coin diameter is 25 mm); (e) deformation structures (scale is 22 cm); and (f) dark shales with horizontal lamination (scale is 10 cm).

distributed within the lower part of the division, but parallel arranged towards the top and middle part of the division (Figure 5b). The massive muddy siltstones contain some plant fragments.

Interpretation: Type A beds are interpreted as the products of debris flows. The massive clean sandstone beds are interpreted as the deposits of poor cohesive debris flows because the sharp contacts with basal and upper mudstones reflect

the plastic rheology of debris flow charge by en masse freezing (Shanmugam, 2013; Talling et al., 2012). The massive clean sandstone beds can also be formed by repeated collapses of traction carpets beneath steady high-density currents or sustained liquefied zones (Talling et al., 2012). Since the stratification structures caused by traction carpets as well as dewatering structures are rare in the type A beds in the study area, the interpretation of the origin of type A beds as poorly

cohesive debris flows is more convincing. The massive muddy siltstone beds are interpreted as the deposits of cohesive debris flows. The sharp contact reflects the plastic rheology of debris flow charge by en masse freezing, while the floating mud clasts indicate that the strength of matrix is high enough to support clasts, which is characteristic of cohesive debris flows (Shanmugam, 2013; Talling et al., 2012).

Type B beds: structured and stratified sandstone beds

Description: Type B bed, usually 0.01–0.5 m thick, are common in both fine-grained clean sandstone and muddy siltstone. In the structured and stratified sandstone beds, normally graded bedding (Figure 5c, d) is the most common sedimentary structure, although ripple cross-beddings and parallel-beddings are also seen (Figure 5c). Normally graded clean sandstones show erosional basal contacts with the underlying mudstones (Figure 5c, d), with commonly developed flame structures (Figure 5c) and flute casts (Figure 4a). Weakly normal-graded bedding muddy siltstones are mainly characterised by thin-bedded normal grading with weak erosional features at the base (Figure 5d).

Interpretation: Type B beds are interpreted as the products of turbidity currents. Normally graded clean sandstones are interpreted as the deposits of high-density turbidity currents because the well-developed stratification in normal grading is indicative of deposition of traction carpets from the high-density flow (Figure 5c) (Postma, Cartigny, & Kleverlaan, 2009; Talling et al., 2012). The strong erosional feature at the base of this sandstone type also indicates the high-energy nature of the flow, typical of high-density turbidity currents (Postma et al., 2009; Talling et al., 2012). Weak normal graded-bedding muddy siltstones are interpreted as the deposits of low-density turbidity currents because the thin-bedded and weak grading indicates the gradual settlement process in relatively low-density turbulent flows (Talling et al., 2012). The rippled sandstones are also the product of low-density turbidity currents and are probably equivalent to the Tc division of Bouma (1962) and Talling et al. (2012).

Type C beds: deformation sandstone and mudstone beds

Description: Type C beds, ranging from 0.1 to 5 m, are composed mainly of muddy siltstones. Soft-sediment deformation structures are common in these beds, in the form of large-scale slump folds (Figure 2g, h), intense mixing of inter-bedded sandstone and mudstone by deformation (Figure 5e), convolute beddings (Zhou et al., 2015b), liquefied deformations and sandy injections (Zhou et al., 2015b), load structures (Zhou et al., 2015b), mud clasts, ball-and-pillow structures (Figure 5e), dewatering structures (Zhou et al., 2015b), syn-sedimentary boudinages (Lu et al., 2011), syn-sedimentary duplexes (Lu et al., 2011) and so on.

Interpretation: Type C beds are interpreted as the products of slumps. The widely distributed soft-sediment deformation structures are interpreted as slumping deformation after primary sediment gravity-flow deposition (Yang & Van Loon, 2016), because many internal structures of

sediment gravity-flow deposits, like normal grading and flute casts, can be observed within soft-sediment deformed deposits.

Type D beds: mud clast-rich bipartite event beds

Description: Type D are mainly observed in Section C (Figure 1c). Individual beds range from 63 to 80 cm, with a mean of 72 cm (Figure 6a, b). According to the differences in lithologies, colours and sedimentary structures, the beds can be divided into two units with a bipartite structure. The lower unit is about 7–20 cm thick, with a mean thickness of 13 cm. The grey and white colours of fine-grained sandstone and siltstone reflect their relatively low mud content. The sandstone is massive. The boundary between the lower unit and underlying mudstone is sharp but without erosional features (Figure 6a, b). In some cases, the boundary between sandstone and mudstone is wavy as the sandstone locally thins (Figure 6a). The upper unit, consists mainly of muddy siltstone, ranging from 50 to 65 cm with a mean of 59 cm. The dark grey colour of the muddy siltstones reflects relatively high mud contents based on petrographic data. Muddy siltstones are massive with ball-and-pillow structures and disorderly floating mud clasts. Some of the mud clasts show a parallel arrangement and are squeezed thin at their margins (Figure 6b). The boundary between the upper unit and overlying mudstone is sharp but without erosional signs, whereas the boundary between the lower and upper unit is sharp without erosion and locally wavy (Figure 6a–c).

Interpretation: Type D beds are interpreted as the products of HEBs caused by particles of cohesive debris flow rearrangement, which means particles above a critical size settle out, whereas smaller particles remain suspended in the flow (Sumner et al., 2009; Talling et al., 2004). This event bed (HEB 1) is dominated by muddy debrite with a thin clean sandstone base. The boundary between the lower clean massive sandstone and the underlying mudstone is sharp without erosion features (Figures 6 and 7). Therefore, the clean sandstones cannot be formed by turbidity currents, which may develop with normal grading and erosional structures (Talling, 2013; Talling et al., 2004). There are some poor cohesive debris flows deposits accompanying HEB 1 (Figure 7d), indicating a relatively proximal setting. It is impossible for HEB 1 to be formed by turbidity current out runs debris flows in a relatively distal setting (Sumner et al., 2009; Talling et al., 2004). The wide distribution of soft-sediment deformation structures and large-scale slumping deposits indicate a sedimentary environment characterised by frequent tectonic movements (Yang & Van Loon, 2016; Zhou et al., 2015a). It is highly possible that the tectonic movement will promote rearrangement of the particles at the base of cohesive debris flows by remobilisation or shocks (Figures 7 and 8a) (Sumner et al., 2009; Talling et al., 2004). Therefore, particles above a critical size will settle out and produce a basal clean sand layer (Figure 9a). Finally, HEB 1 with thick massive muddy debrites emerged with relatively clean massive sandstone bases, and sharp contact boundaries to the upper unit (Figure 9a).

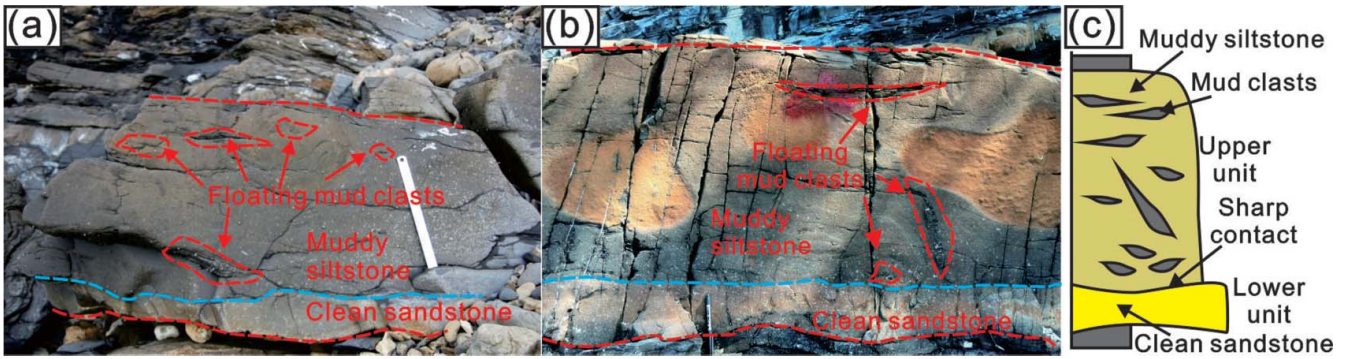


Figure 6. Characteristics of type D beds outcropping on Lingshan Island. (a) Internal structures of bipartite type D bed on the northern end of section C (scale is 22 cm); (b) internal structures of bipartite type D bed in the southern end of section C (14 cm pen for scale); and (c) idealised vertical sequence of type D bed.

Type E beds: mud clast-rich tripartite event beds

Description: Type E beds are mainly observed in Section B (Figure 1c). The type E beds usually range from 10 to 71 cm with a mean of 27 cm. Individual beds can be subdivided into three units with a tripartite structure. The lowest unit, ranging from 3 to 9 cm with a mean of 5 cm, are composed mainly of fine-grained clean sandstone with the overall greyish white colour indicating a low mud content (Figure 10a, b). Pronounced normal grading is well developed in the lower unit (Figures 10a–b and 11a–d). Towards the top of this unit, weak

parallel laminations and water escape structures are developed. The boundary between sandstone and the underlying mudstone is characterised by obviously strong erosion features like flute casts (Figure 10a, b). The middle unit, ranging from 6 to 50 cm with a mean of 16 cm, is composed mainly of muddy siltstones with the dark grey colour reflecting a high mud content. Dark grey floating mud clasts with parallel orientation are present in places in the middle and top parts of the massive muddy siltstones (Figure 10a, b). Some of the mud clasts are almost upright and disorderly distributed in

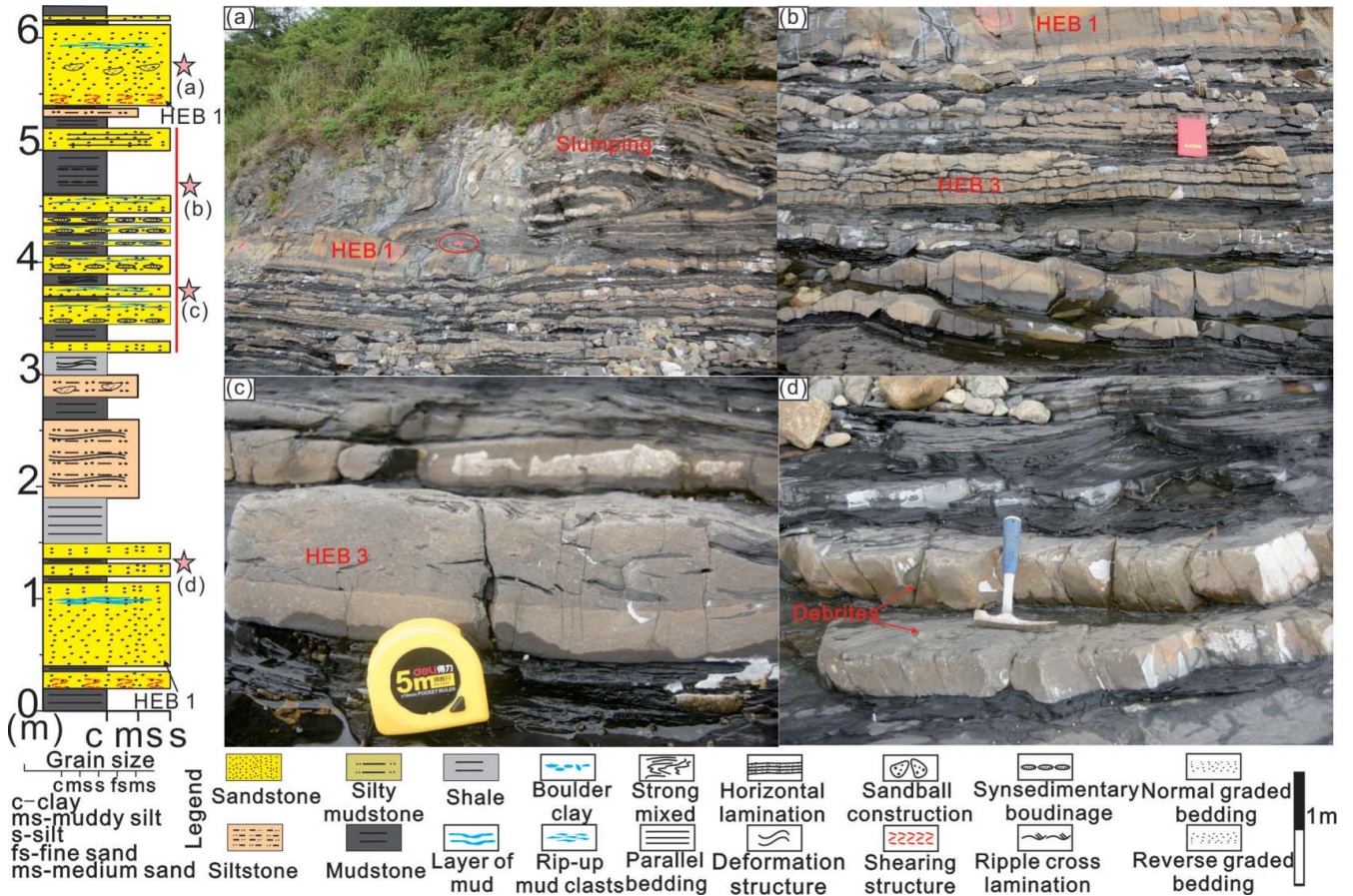


Figure 7. Vertical distribution of type D bed in the section C. (a) Type D bed associated with slumping deposits (notebook for scale is ~20 cm long); (b) location and type D bed associated with type F bed (notebook for scale is ~20 cm long); (c) location and internal structures of type F bed (box for scale is ~5 cm long); and (d) massive clean sandstones associated with type D bed (hammer for scale is ~30 cm long).

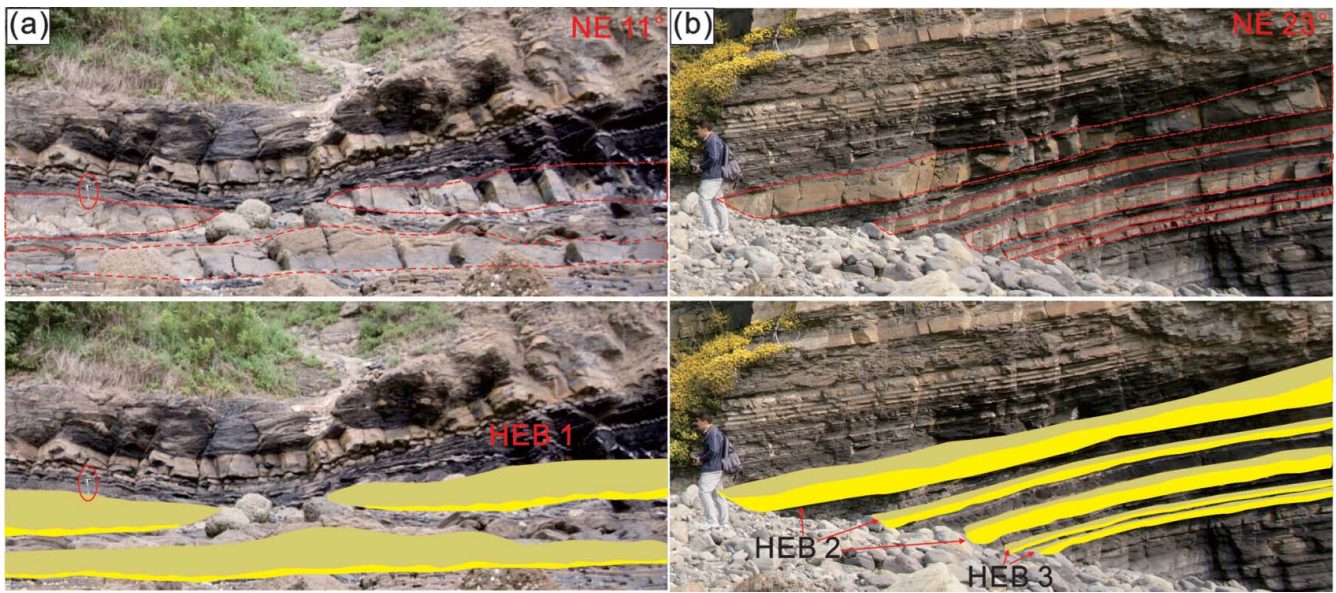


Figure 8. Lateral distribution of different types HEBs on Lingshan Island. (a) Distribution of type D bed, section C (hammer for scale is ~30 cm long); and (b) distribution of type E bed and type F bed, section B (person is ~1.7 m tall). For legend, see Figure 6.

the structureless muddy siltstones (Figure 10a). The top unit, ranging from 1 to 12 cm with a mean of 6 cm, is composed mainly of siltstone and muddy siltstone with relative high mud contents. Weak normal-grading, parallel lamination and horizontal laminations are developed in this unit (Figure 10a). The boundary between the top unit and the overlying

mudstone is gradual, whereas the boundary between the top unit and the middle is always sharp (Figure 10a–c). The boundary between the middle unit and lowest unit is also gradual. The top unit of type E beds may be absent in many cases; thus type E beds are commonly bipartite (Figures 10b and 11a–d).

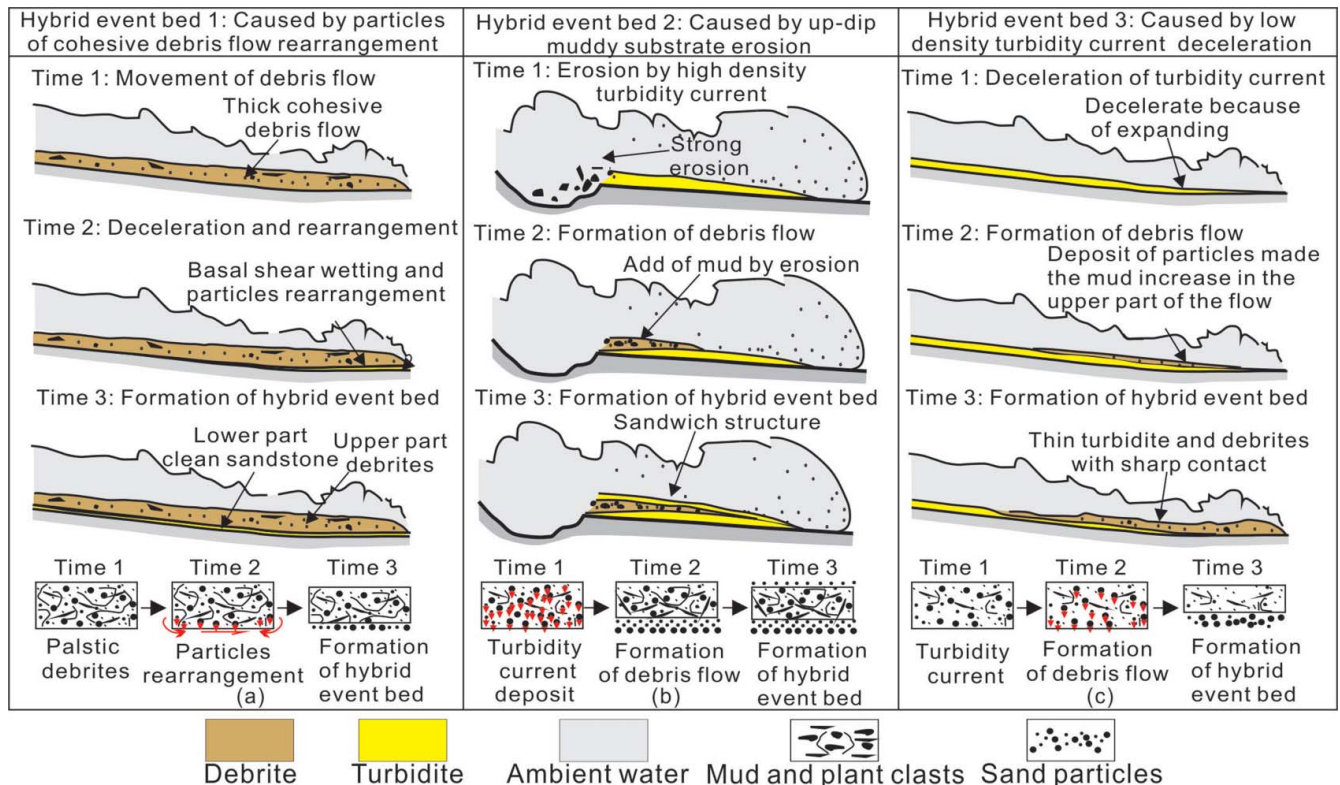


Figure 9. Proposed mechanisms for the origin of deep-water sediment gravity-flow HEBs on Lingshan Island (modified from Haughton et al., 2010; Talling et al., 2004). (a) Type D bed caused by the particles of debris flow rearrangement; (b) type E bed caused by the erosion of basal mud by a high-density turbidity currents; and (c) type F bed caused by the deceleration of a low-density turbidity currents.

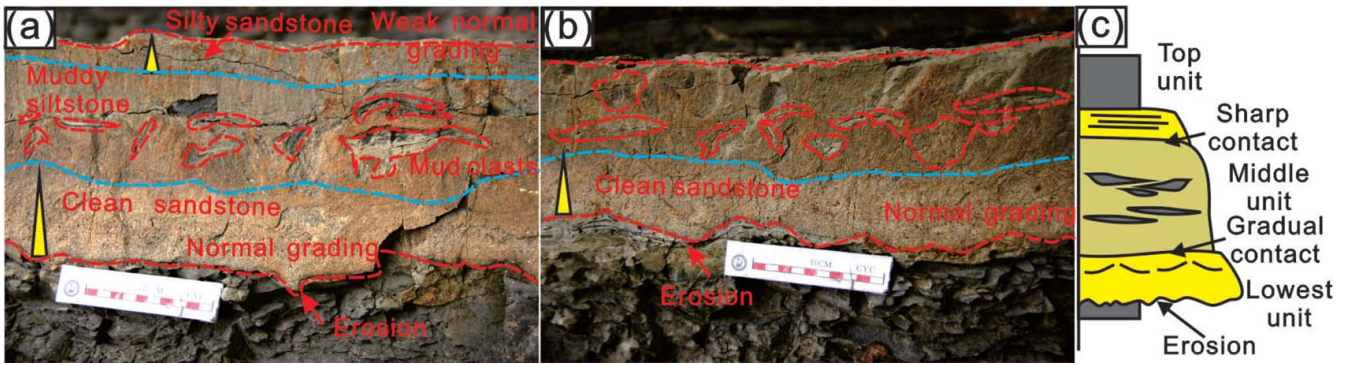


Figure 10. Characteristics of type E bed on Lingshan Island. (a) Internal structures of tripartite type E bed in section B (scale is 10 cm); (b) internal structures of bipartite type E bed in section B (scale is 22 cm); and (c) idealised vertical sequence of type E bed. For legend, see Figure 6.

Interpretation: Type E beds are interpreted as the products of the tripartite structure, as a result of high-density turbidity current deposition (Figures 10b and 11a–d). The erosion of muddy substrates by high-density turbidity currents can cause the incorporation of mud clasts and matrix within the

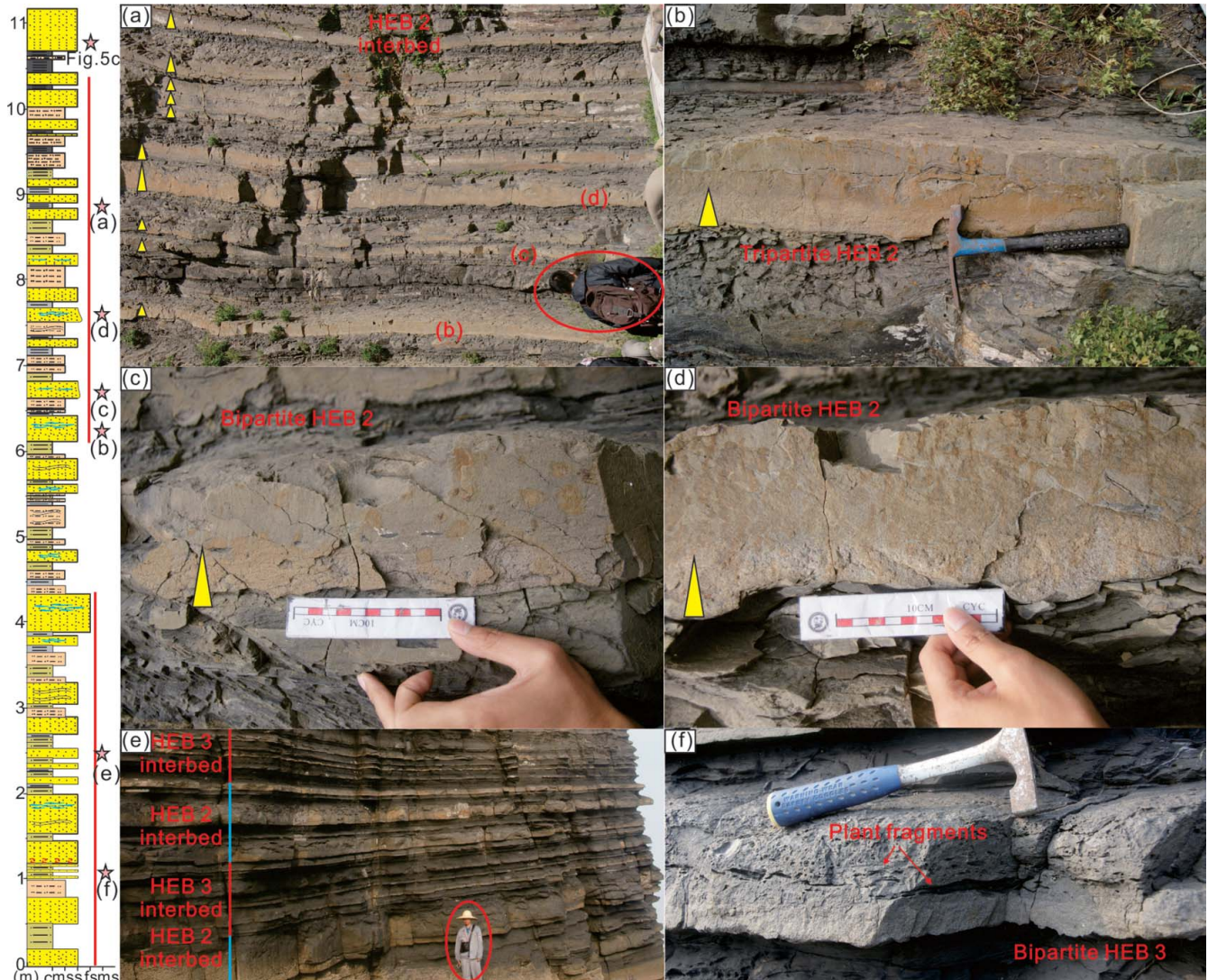


Figure 11. Vertical distribution of type E bed in the section B. (a) Type E bed associated with high-density turbidites (part of a person is ~1 m); (b) location and internal structures of tripartite type E bed (hammer for scale is ~30 cm long); (c) location and internal structures of bipartite type E bed (scale is 10 cm); (d) location and internal structures of bipartite type E bed (scale is 10 cm); (e) location and type E bed interbedded with type F bed (part of a person is ~1.5 m); and (f) location and internal structures of bipartite type F bed (hammer for scale is ~30 cm long). For legend, see Figure 7.

upper part of high-density turbidity current deposits (Haughton et al., 2003, 2009, 2010; Ito, 2008; Kane & Pontén, 2012; Lee et al., 2013; Talling, 2013; Talling et al., 2004). With increasing amounts of mud matrix and mud clasts, turbidity currents transform into debris flows (Sumner et al., 2009; Talling et al., 2004) (Figure 9b). The mud clasts are distributed in the middle part of HEBs 2 by flow partitioning (Haughton et al., 2009, 2010) (Figures 10b and 11a–d). The irregular shape and chaotic distribution of these mud clasts also imply an erosional origin. The lowest unit is emplaced by the frontal part of the high-density turbidity currents, the top unit is the deposition from a trail waning low-concentration and turbulent cloud (Haughton et al., 2009, 2010) (Figures 9b and 10a). Therefore, the deposits of different parts of the flow can form a tripartite structure HEB 2 (Talling et al., 2004) (Figures 9b and 10a). The thickness of the middle part (the debrite) is controlled by the energy of the initial turbidity current and the amount of added mud matrix (Figure 9b). Besides, because of the strong erosive capacity of the lowermost part of the flow (the turbidity current), the top unit of underlying HEB may be partly or completely eroded, to form a bipartite HEB 2 (Figures 10b and 11b–d).

Type F beds: mud clast-poor bipartite event beds

Description: Type F beds are observed in all sediment gravity-flow deposits on the island and are extremely common in Section A (Figure 1c). They are thin-bedded, ranging from 4 to 10 cm with a mean of 6 cm. Individual beds can also be subdivided into two parts according to a bipartite structure (Figure 12a, b). The lower unit is 2–4 cm thick with a mean of 3 cm and is composed mainly of fine-grained sandstone and siltstone with a grey to whitish colour owing to its low mud content. Weak normal-grading is present in this otherwise structureless sandstone (Figure 12a, b). Some weak erosional structures are present in the soles of sandstones (Figure 12b). The boundary between the lower part and its underlying mudstone is sharp (Figure 12a–c). The upper unit, ranging from 1 to 7 cm with a mean of 4 cm, is composed mainly of muddy siltstone. The upper unit is dark grey, reflecting a relatively high mud and carbon content. Abundant plant fragments and occasional mud clasts with parallel arrangement are common in the middle and upper parts of this unit

(Figure 12a, b). The boundary between lower and upper units is sharp without any evidence of erosion (Figures 12 and 13).

Interpretation: Type F beds are interpreted as the products of HEBs caused by low-density turbidity current deceleration. This type of event bed (HEB 3) has a thin thickness and stable lateral distribution (Figures 8b and 13). Normal grading and erosive structures are not common in the lower part, indicating a weak energy regime, typical of low-density turbidity currents (Figures 12 and 13). These features may reflect a low-velocity turbidity current in the late stage of sediment gravity-flow evolution (Southern, Patacci, Felletti, & McCaffrey, 2015) (Figure 9c). The expansion of the late-stage low-velocity turbidity currents leads to the rapid deposition of particles and floating of the mud and plant fragments to the upper part of the flow. The existing mud and plant fragments in turn increase flow viscosity causing the upper part of the flow to transform into debris flows (Haughton et al., 2009, 2010; McCave & Jones, 1988; Talling, 2013). Moreover, the low density and flat plant fragments are easy to float, thus promoting flow transformations (Figures 7c, 11f and 12). When the viscosity of the upper flow reaches the threshold of flow conversion from turbidity current to debris flow (Southern et al., 2015), it will transform fully into a debris flow, which can form the sharp boundary between the upper and lower unit (Figure 9c). The relatively weak energy of the flow results in the thin bed with the late stage of sediment gravity flow always occupying large areas (Talling et al., 2004) and can lead to the stable distribution of HEBs 3 over large areas (Figures 7b, 8b, 11e and 13).

Type G beds: background mudstone beds

Description: Mudstone beds are dominated by horizontal lamination with occasional plant fragments (Figure 5f). These beds form continuous, horizontally laminated stratification with thicknesses of approximately 1 mm (Figure 5f). Mica, clay and organic matter are observed under the microscope to be parallel to the bedding.

Interpretation: The horizontally laminated beds are most likely to have formed through the deposition of background mud by suspension settling. The transportation and deposition from flocculated particles in low-density turbidity

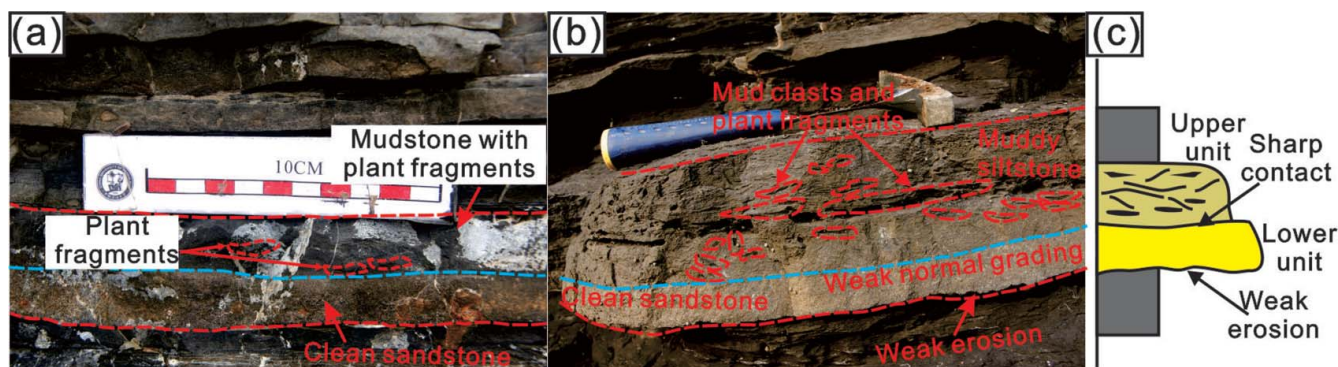


Figure 12. Characteristics of type F bed on Lingshan Island. (a) Internal structures of bipartite type F bed in section A (scale is 10 cm); (b) internal structures of bipartite type F bed in section B (hammer for scale is ~30 cm long); and (c) idealised vertical sequence of type F bed. For legend, see Figure 6.

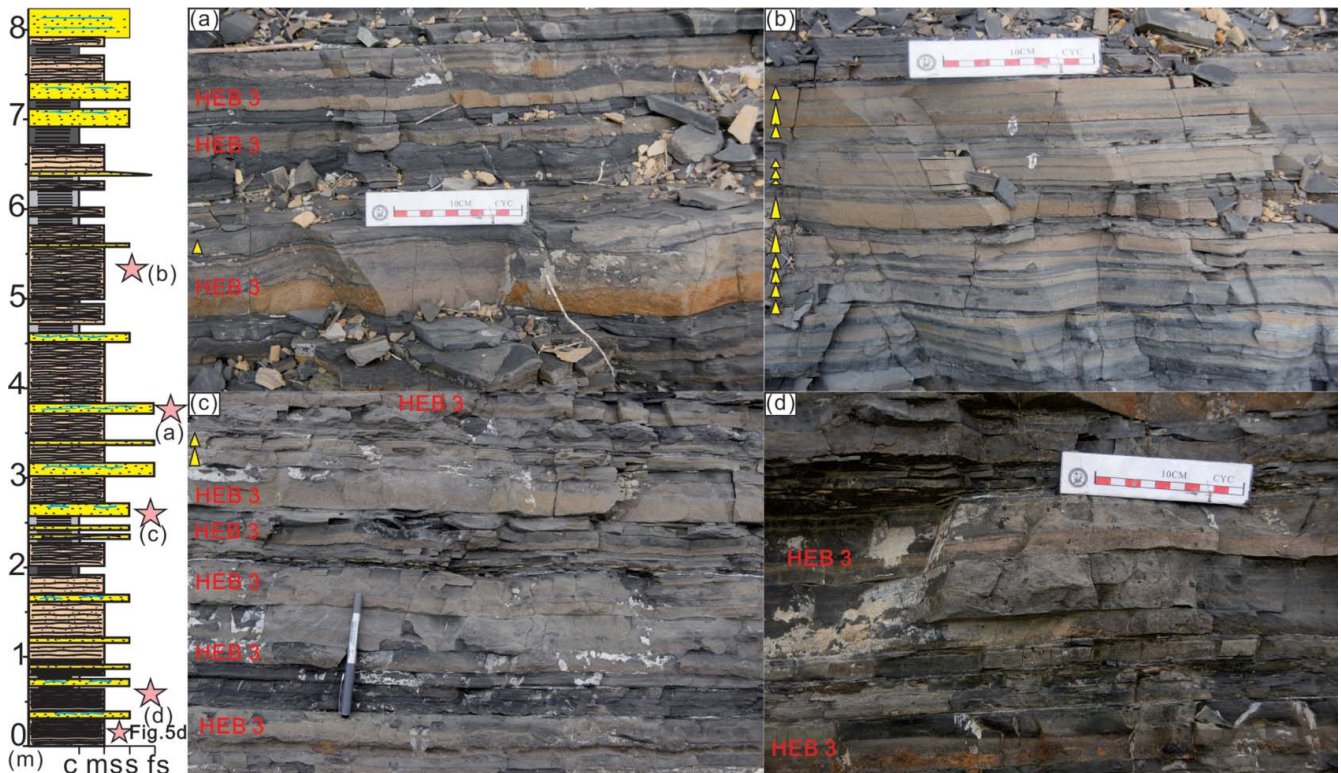


Figure 13. Vertical distribution of type F bed in section A. (a) Internal structures of bipartite type F bed associated with low-density turbidite sandstones (scale is 10 cm); (b) location and thin-bedded normal grading low-density turbidite sandstones interbedded with mudstones (scale is 10 cm); (c) location and type F bed associated with low-density turbidite sandstones (14 cm pen for scale); and (d) location and internal structures of bipartite type F bed (scale is 10 cm). For legend, see Figure 7.

currents are also possible (Talling et al., 2012). Since abundant plant fragments have not been found in this bed, the deposition of prodelta or lofting rhythmites can be ruled out (Zavala & Arcuri, 2016).

Distribution of HEBs

Vertical organisation

Two layers of HEBs 1 are mainly distributed in the south end of the C outcrop section (Figure 7). This section is composed mainly of silty sandstones and muddy sandstones. Silty sandstones account for 30.5%, muddy sandstones account for 45.3%, while mudstones account for 24.2% of the total succession. The thickness of individual beds ranges from 1 to 87 cm. HEBs 1 are accompanied by large-scale slumping deposits and various kinds of soft-sediment deformation structures (Figure 7a). The thin-bedded deposits under HEBs 1 are composed mainly of HEBs 3 with syn-sedimentary boudinages (Figure 7b, c). There are also some massive clean sandstones vertically associated with HEBs 1 (Figure 7d).

A dozen layers of HEBs 2 are mainly distributed in Section B (Figure 11). This section is composed mainly of silty sandstone and muddy sandstone. Silty sandstone accounts for 46.8%, muddy sandstone accounts for 38.6%, and mudstone accounts for 14.6% of the total succession. The thickness of individual beds ranges from 1 to 60 cm, and the beds are laterally continuous (Figures 8b and 11). There are mainly

tripartite HEB 2 and bipartite HEB 2 interbedded in the upper part of the Qiancengya sediment gravity-flow deposit succession with occasionally normally graded-bedding clean sandstones (Figures 5c and 11a–d). In the lower part of Section B gravity-flow-deposit succession, there are mainly interbedded bipartite HEB 2 and bipartite HEB 3 interbedded (Figures 11e, f).

Tens of layers of HEBs 3 are mainly distributed in Section A (Figure 13). This section is composed mainly of muddy sandstones. Muddy sandstones represent 72.5%, silty sandstones represent 17.3%, while mudstones represent 10.2% of the total succession (Figure 13). The thickness of individual beds ranges from 0.1 to 0.5 cm (Figure 13). The bipartite HEB 3 is mainly accompanied by weak normal-graded-bedding muddy siltstones (Figure 13a–d). HEB 3 are thicker than the weak normal-graded-bedding muddy siltstone beds. HEBs 3 are also interbedded with dark shales, which have abundant carbon and plant fragments (Figure 13a, c, d).

Lateral distribution

There are some differences in the lateral distribution feature of the different types of HEBs. HEB 1 is mainly moderately to thickly bedded, structureless sandstone with discontinuously lenses in the upper part of Section C from north to south. On the contrary, HEB 1 in the lower part of Section C forms a continuous bed (Figure 8a). HEBs 2 and 3 are mainly moderately to thinly bedded sandstones and distributed mainly in the A

and B outcrop sections. The sandstones are laterally continuous with only minor changes in thickness along the outcrop section, as illustrated by Section B, where different HEBs in the section that range in thickness from 5 to 60 cm are uniformly distributed over 200 m in the direction of NE 23° (Figure 8b).

Discussion

Distribution patterns of HEBs and sediment gravity-flow evolution processes

HEB 1 is mainly developed in Section C (Figure 7), while HEB 2 is mainly present in Section B (Figure 11). HEB 3 is common in the lower part of Section B, Section C and Section A (Figures 7, 11 and 13). There is a progradational sequence in the Lingshandao Formation from Section A to Section C (Figure 2) (Yang, Fan, Han, & Van Loon, 2016; Yang & Van Loon, 2016; Zhou et al., 2015a). Taking the grey–white rhyolite as a stratigraphic marker (Figure 1c), Section C is close to the grey–white rhyolite compared with the other two sections (Figure 14). There is a conformable contact between the grey–white rhyolite and deep-water sediment gravity-flow deposits without exposure and erosion (Figures 2c and 14a). The obvious small-scale flow structures in the soles of the grey–white rhyolite also imply underwater flow processes (Figure 14a). Thus, the distance between this stratigraphic marker and underlying strata can indicate the relative duration of the formation of different strata. Section A could be coeval with the lower part of Section B and belongs to the lower part of sediment gravity-flow deposits, while Section C could belong to the upper part of sediment gravity-flow deposits (Figures 1c and 14b, c). HEBs 1 in Section C are also accompanied by poor cohesive debris flow deposits (Figure 7). HEBs 2 in Section B are associated with high-density turbidity current deposits (Figure 11), while HEBs 3 in Section A are mainly accompanied by low-density turbidity current deposits (Figure 13). The thickness of sandstone beds increased from Section A towards Section C. Nevertheless, the changing of sediment supply and autogenic controls can also influence the thickness of sandstone beds. The thickness of sandstone beds increased regularly from base to top, providing strong evidence of a prograding succession (Yang et al., 2016)

(Figure 2). Thus, the vertical distribution of these deposits could represent the expression of the longitudinal deposits (*i.e.* Walther's Law; Middleton, 1973), implying HEB evolution processes from HEB 1 to HEB 3 (Figures 2, 7, 11 and 13). The directions of paleoflow are mainly to the southwest, which also corresponds with the evolution of HEB 1 to HEB 3 from northeast to southwest (Figure 1).

Evolution of sediment gravity flows from cohesive debris flows into turbidity currents is well known (Mutti, Ricci Lucchi, & Tinterri, 2009; Talling et al., 2013). The distribution of HEBs together with debrites and turbidites imply a more complicated and continuous evolution process. Following sediment failures or other triggering mechanisms (Piper & Normark, 2009), the semiconsolidated sediment will first evolve into a debris flow (Mutti et al., 2009; Talling et al., 2013). The particle rearrangement of the cohesive debris flows (Sumner et al., 2009) and the differential velocities of turbidity currents and cohesive debris flows (Haughton et al., 2009; Talling, 2013) will result in the development of HEBs, such as HEB 1 in the Lower Cretaceous Lingshandao Formation on Lingshan Island. At the same time, poor cohesive debris flows will transform into high-density turbidity currents by mixing with ambient water (Felix & Peakall, 2006). The erosion of muddy substrate by high-density turbidity currents will then form HEBs as the accumulated HEB 2 in the Lower Cretaceous Lingshandao Formation on Lingshan Island. High-density turbidity currents will be transformed into low-density turbidity currents as the sediment particles settle and diluted with ambient water (Felix & Peakall, 2006). Eventually, the deceleration of low-density turbidity current may form the HEBs as the accumulated HEB 3 in the Lower Cretaceous Lingshandao Formation on Lingshan Island (Figure 15).

Although the accurate situation for HEBs development is still unknown (Fonnesu et al., 2016; Haughton et al., 2009), the occurrences of HEBs allow us to build a more accurate distribution pattern for deep-water sediment gravity-flow sandstones (Figure 15). The development of HEB 1 may imply a relatively proximal setting, the appearance of HEB 2 may represent deposition of high porosity-permeability clean sandstones in the upstream section, deposited by high-density turbidity currents, while the occurrence of HEB 3 represents the potential source rocks and perhaps unconventional reservoirs (Figure 15).

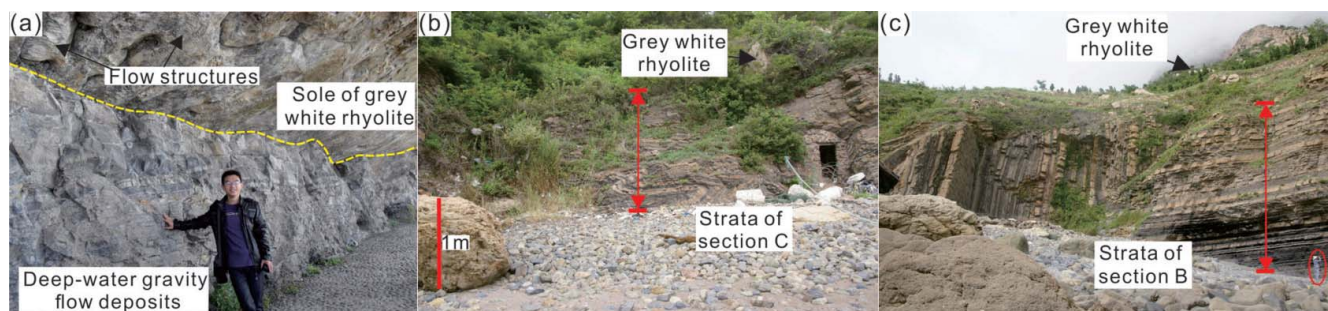


Figure 14. Stratigraphic correlation and trends on Lingshan Island. (a) A conformable contact between grey–white rhyolite and deep-water sediment gravity-flow deposits (part of a person is ~1.2 m); (b) the distance between grey–white rhyolite and deep-water sediment gravity-flow deposits in the section C (scale is 1 m); and (c) the distance between grey–white rhyolite and deep-water sediment gravity-flow deposits in the section B (person is ~1.6 m tall).

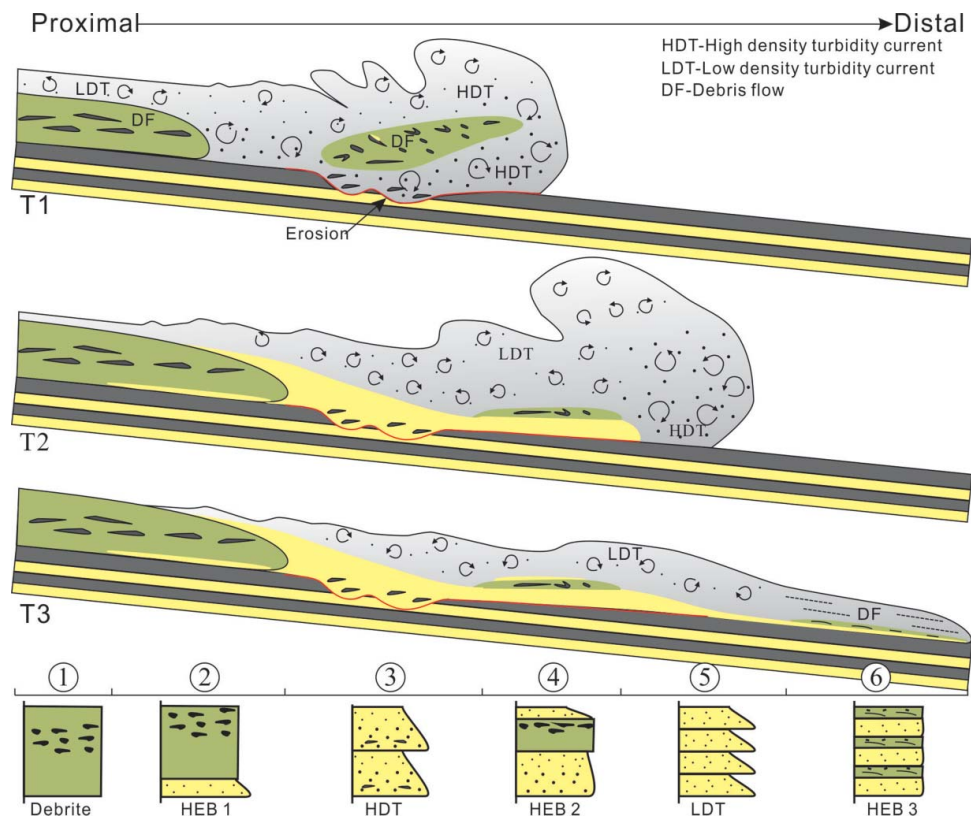


Figure 15. Patterns of deep-water sediment gravity-flow evolution on Lingshan Island. T1, movement of debris flow and the erosion of high-density turbidity current; T2, particle rearrangement at the base of debris flow and the deposition of high-density turbidity current associated with debris flow caused by up-dip muddy substrate erosion; and T3, deposition of low-density turbidity currents and the debris flow caused by low-density turbidity current deceleration.

Comparison with previous models

The distribution pattern of HEBs and sediment gravity-flow evolution processes presented herein are aligned with previous widely cited evolution scheme for deep-water sediment gravity flows (e.g. Barker, Haughton, McCaffrey, Archer, & Hakes, 2008; Fonnesu et al., 2015, 2018; Haughton et al., 2009; Kane & Pontén, 2012; Lowe et al., 2003; Mueller, Patacci, & Di Giulio, 2017; Mutti, 1992; Pierce et al., 2018; Southern et al., 2017; Talling et al., 2004). This study provides new insight into the understanding of sediment gravity-flow evolution processes associated with the genesis of HEBs.

The seminal sediment gravity-flow evolution processes from debris flow to turbidity current provided by Mutti (1992) involves flow dilution owing to the entrainment of ambient water (Haughton et al., 2009; Talling, 2013). The discovery of cohesive debris flow deposits in relatively distal locations may indicate that the temporal flow transformation from turbidity current into debris flow is mainly caused by flow partitioning (Barker et al., 2008; Fonnesu et al., 2015; Haughton et al., 2009; Kane & Pontén, 2012; Lowe et al., 2003; Southern et al., 2017; Talling et al., 2004). Therefore, the overall sediment gravity-flow evolution processes may change from debris flow into turbidity current in the proximal settings and form turbidity current into debris flow in the distal settings (Figure 15). The results of turbidity current transformations into debris flows form distinct HEBs (Haughton et al., 2009;

Talling, 2013). The covering of turbidites by cohesive debris flow deposits, owing to the differential transport velocities or sand settlement from cohesive debris flow deposit after the flow has stopped, via segregation from the muddy suspension can also form HEBs (Sumner et al., 2009; Talling, 2013). Therefore, HEBs caused by different mechanisms may distribute from proximal to distal deep-water sediment gravity-flow deposition settings (Fonnesu et al., 2018; Mueller et al., 2017). Many hypotheses related to the genesis of HEBs have been put forward (Haughton et al., 2009; Talling, 2013) but no studies have discussed the relationship between the genesis and distribution of HEBs with deep-water sediment gravity-flow evolution processes.

Fonnesu et al. (2015, 2018) proposed an evolution process of HEBs from relatively proximal to distal settings and outlined how erosion and incorporation of substrate mud will cause turbulence damping and form HEBs. Thick-bedded HEBs containing large-scale mud clasts may be emplaced into relatively proximal settings. On the contrary, thin-bedded HEBs containing comminuted mud chips and abundant hydraulically separated mica flakes may be emplaced into relatively distal settings (Barker et al., 2008; Fonnesu et al., 2015, 2018; Haughton et al., 2009; Talling, 2013) (Figure 12). We agree with Fonnesu et al. (2015, 2018) that the distribution patterns of HEBs are widespread, and propose that the thinly bedded HEBs in relatively distal

settings may be caused by low-density turbidity current deceleration (Figures 11e, 12 and 13).

Kane and Pontén (2012) and Southern et al. (2017) discussed the evolution of transitional flow deposits (slurry beds) from relatively proximal to distal areas and show that there is an overall reduction in the total thickness, bed amalgamation, sand-to-mud ratio and grain size of banded sandstone beds in distal settings (Southern et al., 2017) (Figure 2). The banded sandstones record progressive deposition of the HEB (Lowe & Guy, 2000; Lowe et al., 2003). Moreover, these authors also indicated that spatial variations of clay-poor sandstone at the base of HEBs may differ depending on the mechanisms by which they are emplaced (Southern et al., 2017). We agree with the notion proposed by Southern et al. (2017) that the geometry of HEBs can indicate their genesis mechanism, and believe that the banded structures of sandstone may reflect the vertical stacking pattern of numerous HEBs (Figures 7, 9, 10 and 12).

The observations made here show that the geometry of HEBs indicate their genesis mechanisms (Fonnesu et al., 2015; Kane & Pontén, 2012; Southern et al., 2017), as well as the distribution patterns of HEBs (Fonnesu et al., 2015, 2018; Haughton et al., 2003). Therefore, the genesis of HEBs in the Lower Cretaceous Lingshan Island can be estimated based on the thickness, sedimentary structures and contact relationships among the different units. The distribution of HEBs together with debrites and turbidites implies a continuous evolution process of deep-water sediment gravity flows (Pierce et al., 2018), which supplement deep-water sediment gravity-flow evolution processes.

Significance

Deep-water sediment gravity flows are notoriously difficult to monitor directly, owing to their unpredictable occurrence and their ability to destroy monitoring equipment (Talling et al., 2015), and this is the fundamental reason for the uncertainties in deep-water sediment gravity-flow research (Shanmugam, 2013; Talling et al., 2012, 2013, 2015). The findings of HEBs in the Lower Cretaceous outcrop sections on the Lingshan Island provide evidence that HEBs are widespread in both marine and lacustrine deep-water environments worldwide (Talling et al., 2015). This means that with regard to the related deep-water sediment gravity-flow models (e.g. Kuenen & Migliorini, 1950; Mutti et al., 2009; Shanmugam, 2013; Talling et al., 2013) although presently widely accepted, there are still difficulties in explaining the origin and distribution patterns of many deep-water sediment gravity-flow deposits. The understanding of deep-water sediment gravity-flow deposits and their distribution is still limited. The forecasting based on deep-water sediment gravity-flow deposition forecasting build by flow dilution needs improvement (Haughton et al., 2003, 2009; Talling, 2013; Talling et al., 2004).

The formation and distribution of HEBs are closely related to tectonic activities in a basin (Haughton et al., 2003, 2009). Lingshan Island, which is located in the Sulu orogenic belt, allows analysis of the types and distribution of HEBs to

provide new insights into the tectonic evolution of this area (Wang et al., 2014b), because HEBs deposits are mostly related to distal basin-plain settings (Haughton et al., 2003, 2009; Talling, 2013; Talling et al., 2004).

The HEBs, particularly HEB 3, are commonly distributed in the centre of the deep-water basin (e.g. Haughton et al., 2003, 2009; Lowe & Guy, 2000; Lowe et al., 2003; Talling, 2013; Talling et al., 2004). The process of turbidity current transformation into debris flow may be one important mechanism for fine-grained sediment transportation into the deep-water basin (Hovikoski et al., 2016). Thus, the genesis and distribution of HEBs could be helpful for understanding the origin and distribution of unconventional reservoirs (Galy et al., 2007; Hovikoski et al., 2016; Yang, Cao, Wang, Li, & Zhang, 2015).

Conclusions

Three types of HEBs in the deep-water sediment gravity-flow deposition have been distinguished in the Cretaceous sediment sequence on Lingshan Island, Yellow Sea, China. The type D beds range from 63 to 80, cm with a mean of 72 cm, and can be divided into two units. The lower unit was interpreted as a turbidite, while the upper unit was interpreted as a muddy debrite. The type E beds range from 10 to 71 cm, with a mean of 26.57 cm, and can be divided into three units. The lowest unit was interpreted as accumulated by a high-density turbidite, the middle unit as a muddy debrite and the top unit as low-density turbidite. The type F beds range from 4 to 10 cm, with a mean of 6.46 cm, and can be divided into two units. The lower unit was interpreted as accumulated by a low-density turbidite, and the upper unit as a muddy debrite.

HEB 1 was formed from the remobilisation or shock in the base of cohesive debris flows leading to the rearrangement of the sediment particles. HEB 2 was developed by the erosion of muddy substrate by high-density turbidity currents, which transformed into debris flows owing to the incorporation of mud clasts and mud matrix. HEB 3 was formed by the expansion and decelerating of low-density turbidity currents, which transformed into debris flows.

The distribution of HEBs together with debrites and turbidites implies a continuous evolution process of deep-water sediment gravity flows. The semiconsolidated sediment may first develop into a cohesive debris flow, where the particle rearrangement of the cohesive debris flows form HEB 1. Poor cohesive debris flow may transform into a high-density turbidity current, and the erosion of muddy substrate by the high-density turbidity current to form HEB 2. When the high-density turbidity current transforms into low-density turbidity current, the deceleration of low-density turbidity current forms HEB 3.

Acknowledgements

Dr Zhenkai Zhang is thanked for his beneficial suggestions. Carlos Zavala and an anonymous reviewer are thanked for their constructive comments.

Disclosure statement


No potential conflict of interest was reported by the authors.


Funding

This work was supported by the National Science Foundation of China [grant number U1762217]; China Postdoctoral Science Foundation [grant number 2017M622314]; Chinese Scholarship Council [grant number 201506450029]; National Science and Technology Special Grant [grant number 2016ZX05006-003]; and Qingdao Postdoctoral researcher applied research project [grant number BY20170202].

ORCID

T. Yang  <http://orcid.org/0000-0003-0400-4503>

Y. Cao  <http://orcid.org/0000-0003-0614-4665>

K. Liu  <http://orcid.org/0000-0002-8741-9802>

References

- Amy, L. A., Peachey, S. A., Gardiner, A. A., & Talling, P. J. (2009). Prediction of hydrocarbon recovery from turbidite sandstones with linked-debrite facies: Numerical flow-simulation studies. *Marine and Petroleum Geology*, 26, 2032–2043.
- Baas, J. H., Best, J. L., Peakall, J., & Wang, M. (2009). A phase diagram for turbulent, transitional, and laminar clay suspension flows. *Journal of Sedimentary Research*, 79, 162–183.
- Baas, J. H., Best, J. L., & Peakall, J. (2011). Depositional processes, bedform development and hybrid bed formation in rapidly decelerated cohesive (mud–sand) sediment flows. *Sedimentology*, 58, 1953–1987.
- Barker, S. P., Haughton, P. D. W., McCaffrey, W. D., Archer, S. G., & Hakes, B. (2008). Development of rheological heterogeneity in clay-rich high-density turbidity currents: Aptian Britannia Sandstone Member, U.K. Continental Shelf. *Journal of Sedimentary Research*, 78, 45–68.
- Bouma, A. H. (1962). *Sedimentology of some flysch deposits: A graphic approach to facies interpretation*. Amsterdam: Elsevier, 168 p.
- Dong, X. P., Lu, H. B., Zhang, X., Zhang, H. C., Wang, J., & Zhang, S. J. (2013). Stage analysis on the soft-sediment deformation in the Early Cretaceous Flysch, Lingshan Island, Shandong Province. *Geological Review*, 59, 1060–1067 (In Chinese with English abstract).
- Felix, M., Leszczyński, S., Ślącza, A., Uchman, A., Amy, L., & Peakall, J. (2009). Field expressions of the transformation of debris flows into turbidity currents, with examples from the Polish Carpathians and the French Maritime Alps. *Marine and Petroleum Geology*, 26, 2011–2020.
- Felix, M., & Peakall, J. (2006). Transformation of debris flows into turbidity currents: Mechanisms inferred from laboratory experiments. *Sedimentology*, 53, 107–123.
- Fonnesu, M., Felletti, F., Haughton, P. D. W., Patacci, M., & McCaffrey, W. D. (2018). Hybrid event bed character and distribution linked to turbidite system subenvironments: The North Apennine Gottero Sandstone (north-west Italy). *Sedimentology*, 65, 151–190.
- Fonnesu, M., Haughton, P., Felletti, F., & McCaffrey, W. (2015). Short length-scale variability of hybrid event beds and its applied significance. *Marine and Petroleum Geology*, 67, 583–603.
- Fonnesu, M., Patacci, M., Haughton, P. D. W., Felletti, F., & McCaffrey, W. D. (2016). Hybrid event beds generated by local substrate delamination on a confined-basin floor. *Journal of Sedimentary Research*, 86, 929–943.
- Galy, V., France-Lanord, C., Beyssac, O., Faure, P., Kudrass, H., & Palhol, F. (2007). Efficient organic carbon burial in the Bengal fan sustained by the Himalayan erosional system. *Nature*, 450, 407–410.
- Ge, L. Z., Zhong, J. H., Fan, X. F., Ren, Q. Q., & Shao, Z. F. (2015). Study on internal sedimentary and structural features of the slump body on Lingshan Island, Qingdao, Shandong. *Geological Review*, 61, 634–644 (In Chinese with English abstract).
- Georgiopoulou, A., Wynn, R. B., Masson, D. G., & Frenz, M. (2009). Linked turbidite–debrite resulting from recent Sahara Slide headwall reactivation. *Marine and Petroleum Geology*, 26, 2021–2031.
- Hampton, M. A. (1972). The role of subaqueous debris flow in generating. *Journal of Sedimentary Petrology*, 42, 775–793.
- Haughton, P. D. W., Barker, S. M., & McCaffrey, W. D. (2003). ‘Linked’ debrites in sand-rich turbidite systems—origin and significance. *Sedimentology*, 50, 459–482.
- Haughton, P., Davis, C., McCaffrey, W., & Barker, S. (2009). Hybrid sediment gravity flow deposits – classification, origin and significance. *Marine and Petroleum Geology*, 26, 1900–1918.
- Haughton, P., Davis, C., McCaffrey, W., & Barker, S. (2010). Reply to comment by R. Higgs on ‘Hybrid sediment gravity flows – classification, origin and significance’. *Marine and Petroleum Geology*, 27, 2066–2069.
- Higgs, R. (2010). Comments on ‘Hybrid sediment gravity flows – classification, origin and significance’ from Haughton, Davis, McCaffrey and Barker (Marine and Petroleum Geology, 2009, 26, 1900–1918). *Marine and Petroleum Geology*, 27, 2062–2065.
- Hovikoski, J., Therkelsen, J., Nielsen, L. H., Bojesen-Koefoed, J. A., Nytoft, H. P., Petersen, H. I., ... Fyhn, M. B. W. (2016). Density-flow deposition in a fresh-water lacustrine rift basin, Paleogene Bach Long Vi Graben, Vietnam. *Journal of Sedimentary Research*, 86, 982–1007.
- Ito, M. (2008). Downfan transformation from turbidity currents to debris flows at a channel-to-lobe transitional zone: The Lower Pleistocene Otadai Formation, Boso Peninsula, Japan. *Journal of Sedimentary Research*, 78, 668–682.
- Jackson, C. A. L., Zakaria, A. A., Johnson, H. D., Tongkul, F., & Crevello, P. D. (2009). Sedimentology, stratigraphic occurrence and origin of linked debrites in the West Crocker Formation (Oligo-Miocene), Sabah, NW Borneo. *Marine and Petroleum Geology*, 26, 1957–1973.
- Kane, I. A., & Pontén, A. S. M. (2012). Submarine transitional flow deposits in the Paleogene Gulf of Mexico. *Geology*, 40, 1119–1122.
- Kuenen, P. H., & Migliorini, C. I. (1950). Turbidity currents as a cause of graded bedding. *The Journal of Geology*, 58, 91–127.
- Lee, S. H., Jung, W.-Y., Bahk, J. J., Gardner, J. M., Kim, J. K., & Lee, S. H. (2013). Depositional features of co-genetic turbidite–debrite beds and possible mechanisms for their formation in distal lobated bodies beyond the base-of-slope, Ulleung Basin, East Sea (Japan Sea). *Marine Geology*, 346, 124–140.
- Li, S. J., Zhang, X. Y., Zhao, X. L., Sun, Z. X., Zhang, D. Y., Zhang, L., ... Liu, B. M. (2017). Discovery of fish and conchostracan fossils in Lower Cretaceous in Lingshan Island, Qingdao, Shandong. *Geological Review*, 63, 1–6 (In Chinese with English abstract).
- Lowe, D. R., & Guy, M. (2000). Slurry-flow deposits in the Britannia Formation (Lower Cretaceous), North Sea: A new perspective on the turbidity current and debris flow problem. *Sedimentology*, 47, 31–70.
- Lowe, D. R., Guy, M., & Palfrey, A. (2003). Facies of slurry-flow deposits, Britannia Formation (Lower Cretaceous), North Sea: Implications for flow evolution and deposit geometry. *Sedimentology*, 50, 45–80.
- Lu, H. B., Wang, J., & Zhang, H. C. (2011). Discovery of the late Mesozoic slump beds on Lingshan Island, Shandong, and a pilot research on the regional tectonics. *Acta Geologica Sinica*, 85, 938–946 (In Chinese with English abstract).
- Lu, H. B., Zhang, H. C., Wang, J., Zhang, S. J., Dong, X. P., & Zhang, X. (2013). The answer for Professor Zhong Jianhua – The Early Cretaceous flysch on Lingshan Island are not intracontinental delta deposits. *Geological Review*, 59, 11–14 (In Chinese).
- Luan, G. Z., Li, A. L., Wang, J., Li, G., & Xie, R. J. (2010). The geological origin division of the Main Sea Island in Qingdao Area and environment analysis. *Periodical of Ocean University of China*, 40, 111–116 (In Chinese with English abstract).
- McCaffrey, W., & Kneller, B. (2001). Process controls on the development of stratigraphic trap potential on the margins of confined turbidite systems and aids to reservoir evaluation. *AAPG Bulletin*, 85, 971–988.
- McCave, I. N., & Jones, K. P. N. (1988). Deposition of ungraded muds from high-density non-turbulent turbidity currents. *Nature*, 333, 250–252.
- Middleton, G. V. (1973). Johannes Walther’s law of the correlation of facies. *Geological Society of America Bulletin*, 84, 979–988.

- Mueller, P., Patacci, M., & Di Giulio, A. (2017). Hybrid event beds in the proximal to distal extensive lobe domain of the coarsegrained and sand-rich Bordighera turbidite system (NW Italy). *Marine and Petroleum Geology*, *86*, 908–931.
- Mulder, T., & Alexander, J. (2001). The physical character of subaqueous sedimentary density flows and their deposits. *Sedimentology*, *48*, 269–299.
- Mutti, E. (1992). *Turbidite Sandstones*. San Donato Milanese: Istituto di Geologia Università di Parma & AGIP, 275 p.
- Mutti, E., Ricci Lucchi, F., & Tinterri, R. (2009). Turbidites and turbidity currents from Alpine 'flysch' to the exploration of continental margins. *Sedimentology*, *56*, 267–318.
- Mutti, E., Tinterri, R., Benevelli, G., Biase, D., & Cavanna, G. (2003). Deltaic, mixed and turbidite sedimentation of ancient foreland basins. *Marine and Petroleum Geology*, *20*, 733–755.
- Mutti, E., Tinterri, R., Remacha, E., & Fava, L. (1999). An Introduction to the analysis of ancient turbidite basins from an outcrop perspective. *AAPG Course Notes*, *39* (93 p.). Tulsa OK: AAPG.
- Patacci, M., Haughton, P. D. W., & McCaffrey, W. D. (2014). Rheological complexity in sediment gravity flows forced to decelerate against a confining slope, Braux, SE France. *Journal of Sedimentary Research*, *84*, 270–277.
- Pierce, C. S., Haughton, P. D. W., Shannon, P. M., Pulham, A. J., Barker, S. P., & Martinsen, O. J. (2018). Variable character and diverse origin of hybrid event beds in a sandy submarine fan system, Pennsylvanian Ross Sandstone Formation, western Ireland. *Sedimentology*. Retrieved from <https://doi.org/10.1111/sed.12412>
- Piper, D. J. W., & Normark, W. R. (2009). Processes that initiate turbidity currents and their influence on turbidites: A marine geology perspective. *Journal of Sedimentary Research*, *79*, 347–362.
- Postma, G., Cartigny, M., & Kleverlaan, K. (2009). Structureless, coarse-tail graded Bouma Ta formed by internal hydraulic jump of the turbidity current? *Sedimentary Geology*, *219*, 1–6.
- Pritchard, D., & Gladstone, C. (2009). Reversing buoyancy in turbidity currents: Developing a hypothesis for flow transformation and for deposit facies and architecture. *Marine and Petroleum Geology*, *26*, 1997–2010.
- Shanmugam, G. (2013). New perspectives on deep-water sandstones: Implications. *Petroleum Exploration and Development*, *40*, 316–324.
- Shao, Z. F., Zhong, J. H., Li, Y., Mao, C., Liu, S. X., Ni, N. T., ... Lin, G. S. (2014a). Characteristics and sedimentary processes of lamina-controlled sand-particle imbricate structure in deposits on Lingshan Island, Qingdao, China. *Science China: Earth Sciences*, *57*, 1061–1076.
- Shao, Z. F., Zhong, J. H., Li, Y., Ni, N. T., Liu, S. X., Fan, L. H., & Chen, B. (2014b). The sedimentary characteristics and environmental analysis of late Mesozoic gravity flows on Lingshan Island. *Geological Review*, *60*, 555–566 (In Chinese with English abstract).
- Southern, S. J., Kane, I. A., Warchol, M. J., Porten, K. W., & McCaffrey, W. D. (2017). Hybrid event beds dominated by transitional-flow facies: Character, distribution and significance in the Maastrichtian Springer Formation, north-west Vøring Basin, Norwegian Sea. *Sedimentology*, *64*, 747–776.
- Southern, S. J., Patacci, M., Felletti, F., & McCaffrey, W. D. (2015). Influence of flow containment and substrate entrainment upon sandy hybrid event beds containing a co-genetic mud-clast-rich division. *Sedimentary Geology*, *321*, 105–122.
- Stow, D. A. V., & Johansson, M. (2000). Deep-water massive sands: Nature, origin and hydrocarbon implications. *Marine and Petroleum Geology*, *17*, 145–174.
- Stow, D. A. V., & Mayall, M. (2000). Deep-water sedimentary systems: New models for the 21st century. *Marine and Petroleum Geology*, *17*, 125–135.
- Sumner, E. J., Talling, P. J., & Amy, L. A. (2009). Deposits of flows transitional between turbidity current and debris flow. *Geology*, *37*, 991–994.
- Talling, P. J. (2013). Hybrid submarine flows comprising turbidity current and cohesive debris flow: Deposits, theoretical and experimental analyses, and generalized models. *Geosphere*, *9*, 460–488.
- Talling, P. J., Allin, J., Armitage, D. A., Arnott, R. W. C., Cartigny, M. J. B., Clare, M. A., ... Xu, J. (2015). Key future directions for research on turbidity currents and their deposits. *Journal of Sedimentary Research*, *85*, 153–169.
- Talling, P. J., Amy, L. A., Wynn, R. B., Peakall, J., & Robinson, M. (2004). Beds comprising debrite sandwiched within co-genetic turbidite: Origin and widespread occurrence in distal depositional environments. *Sedimentology*, *51*, 163–194.
- Talling, P. J., Masson, D. G., Sumner, E. J., & Malgesini, G. (2012). Subaqueous sediment density flows: Depositional processes and deposit types. *Sedimentology*, *59*, 1937–2003.
- Talling, P. J., Paull, C. K., & Piper, D. J. W. (2013). How are subaqueous sediment density flows triggered, what is their internal structure and how does it evolve? Direct observations from monitoring of active flows. *Earth-Science Reviews*, *125*, 244–287.
- Talling, P. J., Wynn, R. B., Masson, D. G., Frenz, M., Cronin, B. T., Schiebel, R., ... Amy, L. A. (2007). Onset of submarine debris flow deposition far from original giant landslide. *Nature*, *450*, 541–544.
- Tinterri, R., & Muzzi Magalhaes, P. (2011). Synsedimentary structural control on foredeep turbidites: An example from Miocene Marnoso-arenacea Formation, Northern Apennines, Italy. *Marine and Petroleum Geology*, *28*, 629–657.
- Wang, A. D., Zhou, Y. Q., Zhang, Z. K., Yu, S. S., & Wang, Z. Y. (2014a). Characteristics and significance of underwater non-tectonic cracks in Laiyang Group of Lingshan Island, Shandong Province. *Acta Geoscientia Sinica*, *35*, 321–328 (In Chinese with English abstract).
- Wang, J., Chang, S. C., Lu, H. B., & Zhang, H. C. (2014b). Detrital zircon U–Pb age constraints on Cretaceous sedimentary rocks of Lingshan Island and implications for tectonic evolution of Eastern Shandong, North China. *Journal of Asian Earth Sciences*, *96*, 27–45.
- Wood, A., & Smith, A. J. (1959). The sedimentation and sedimentary history of the Aberystwyth Grits (Upper Llandoveryan). *Quarterly Journal of the Geological Society of London*, *114*, 163–195.
- Yang, T., Cao, Y. C., Wang, Y. Z., Li, Y., & Zhang, S. M. (2015). Status and trends in research on deep-water gravity flow deposits. *Acta Geologica Sinica (English Edition)*, *89*, 610–631.
- Yang, R. C., Fan, A. P., Han, Z. Z., & Van Loon, A. J. (2016). An upward shallowing succession of gravity flow deposits in the Early Cretaceous Lingshanda Formation, Western Yellow Sea. *Acta Geologica Sinica*, *90*, 1553–1554.
- Yang, R. C., Fan, A. P., Han, Z. Z., & Van Loon, A. J. (2017b). Lithofacies and origin of the Late Triassic muddy gravity-flow deposits in the Ordos Basin, central China. *Marine and Petroleum Geology*, *85*, 194–219.
- Yang, R. C., Fan, A. P., Han, Z. Z., & Van Loon, A. J. (2017c). A marine or continental nature of the deltas in the Early Cretaceous Lingshanda Formation — Evidences from trace elements. *Acta Geologica Sinica (English Edition)*, *91*, 367–368.
- Yang, R. C., Jin, Z. J., Van Loon, A. J., Han, Z. Z., & Fan, A. P. (2017a). Climatic and tectonic controls of lacustrine hyperpynite origination in the Late Triassic Ordos Basin, central China: Implications for unconventional petroleum development. *AAPG Bulletin*, *101*(1), 95–117.
- Yang, R. C., & Van Loon, A. J. (2016). Early Cretaceous slumps and turbidites with peculiar soft-sediment deformation structures on Lingshan Island (Qingdao, China) indicating a tensional tectonic regime. *Journal of Asian Earth Sciences*, *129*, 206–219.
- Zavala, C., & Arcuri, M. (2016). Intra-basinal and extrabasinal turbidites: Origin and distinctive characteristics. *Sedimentary Geology*, *337*, 36–54.
- Zhang, H. C., Lu, H. B., Li, J. G., Wang, J., Zhang, S. J., Dong, X. P., ... Reng, X. M. (2013). The Lingshanda Formation: A new lithostratigraphic unit of the Early Cretaceous In Qingdao, Shandong, China. *Journal of Stratigraphy*, *37*, 216–222 (In Chinese with English abstract).
- Zhong, J. H. (2012). The discuss with Professor Lu Hongbo – The Mesozoic deposition on Lingshan Island are deep-water turbidite or intracontinental delta deposits? *Geological Review*, *58*, 1180–1182 (In Chinese).
- Zhong, J. H., Ni, L. T., Shao, Z. F., Li, Y., Liu, X., Mao, C., ... Xiong, Z. Q. (2016). Tempestites and storm deposits in the Lower Cretaceous from Lingshan Island, Qingdao. *Journal of Palaeogeography*, *18*, 381–398 (In Chinese with English abstract).
- Zhou, Y. Q., Zhang, Z. K., Liang, W. D., Li, S., & Yue, H. W. (2015a). Late Mesozoic tectono-magmatic activities and prototype basin restoration in Eastern Shandong Province, China. *Earth Science Frontiers*, *22*, 137–156 (In Chinese with English abstract).
- Zhou, Y. Q., Zhang, Z. K., Xu, H., Wang, A. D., Wei, K., Zhang, Y. C., ... Gao, X. J. (2015b). Soft-sediment deformation structures in the sediments at Lingshan Island. *Marine Geology Frontiers*, *31*, 42–54 (In Chinese with English abstract).